



**HAL**  
open science

## Photoelectrochemical reactors for treatment of water and wastewater:

Emmanuel Mousset, Dionysios Dionysiou

► **To cite this version:**

Emmanuel Mousset, Dionysios Dionysiou. Photoelectrochemical reactors for treatment of water and wastewater:.. *Environmental Chemistry Letters*, 2020, 18 (4), pp.1301-1318. <10.1007/s10311-020-01014-9>. <hal-02993264>

**HAL Id: hal-02993264**

**<https://hal.science/hal-02993264v1>**

Submitted on 5 Dec 2020

**HAL** is a multi-disciplinary open access archive for the deposit and dissemination of scientific research documents, whether they are published or not. The documents may come from teaching and research institutions in France or abroad, or from public or private research centers.

L'archive ouverte pluridisciplinaire **HAL**, est destinée au dépôt et à la diffusion de documents scientifiques de niveau recherche, publiés ou non, émanant des établissements d'enseignement et de recherche français ou étrangers, des laboratoires publics ou privés.



HAL Authorization

1 **Photo-Electrochemical Reactors for Treatment of Water**  
2 **and Wastewater**

3  
4 **Emmanuel Mousset<sup>1,\*</sup> and Dionysios D. Dionysiou<sup>2,\*</sup>**

5  
6 <sup>1</sup> Laboratoire Réactions et Génie des Procédés, Université de Lorraine, CNRS, LRGP, F-  
7 54000 Nancy, France

8 <sup>2</sup> Environmental Engineering and Science Program, Department of Chemical and  
9 Environmental Engineering, 705 Engineering Research Center, University of Cincinnati,  
10 Cincinnati, OH 45221-0012, USA

11  
12  
13  
14 **REVIEW PAPER**

15 ***ENVIRONMENTAL CHEMISTRY LETTERS***

16  
17  
18  
19  
20  
21  
22  
23 Corresponding authors:

24 E. Mousset (✉)

25 Laboratoire Réactions et Génie des Procédés, Université de Lorraine, CNRS, LRGP, F-54000 Nancy, France  
26 email: [emmanuel.mousset@univ-lorraine.fr](mailto:emmanuel.mousset@univ-lorraine.fr)

27  
28 D.D. Dionysiou (✉)

29 Environmental Engineering and Science Program, Department of Chemical and Environmental Engineering, 705  
30 Engineering Research Center, University of Cincinnati, Cincinnati, OH 45221-0012, USA  
31 email: [dionysios.d.dionysiou@uc.edu](mailto:dionysios.d.dionysiou@uc.edu)

## 32 **Abstract**

33 To address the increasing global water demand in parallel to water scarcity, especially  
34 exacerbated by the climate change, the “Water Reuse” option is more and more considered. It  
35 consists of the reuse of water for different sectors with different water quality requirement such  
36 as industry, agriculture and even for human consumption. The biotechnologies currently  
37 implemented are usually cheaper but are not sufficient to completely remove biorecalcitrant  
38 pollution. Advanced oxidation technologies for wastewater treatment have gained significant  
39 interests the last few years as an answer to this issue by producing very strong oxidizing agent  
40 such as hydroxyl radical ( $\cdot\text{OH}$ ) in mild conditions. Electrochemical advanced oxidation  
41 processes have attracted particular attention for water treatment through the continuous and *in*  
42 *situ* electro-catalytic generation of strong oxidizing species under mild conditions with the  
43 possibility to avoid the external addition of chemicals. The synergy between photochemical  
44 systems and electrolysis has more recently seen increasing interest considering benefits from  
45 using solar light as a free energy source. However, there is a lack of literature review on the  
46 reactions and engineering aspects of the photo-electrochemical reactors that play a paramount  
47 role on the overall process efficiency.

48 In this context, we reviewed the trends of photo-electrochemical reactors through two major  
49 points. Firstly, the reactions involved were presented along with the possible synergetic  
50 mechanisms. Under maximal conditions, eight  $\cdot\text{OH}$  production sites could be identified when  
51 implementing photoelectro-Fenton combined with photoanodic oxidation and photocatalysis or  
52 photoelectrocatalysis. Several factors affect the occurrence of these reactions such as the  
53 solution pH, the applied wavelength, and the competition between reactions requiring the same  
54 reagent. Secondly, the different reactor design developed in response to the catalytic  
55 phenomena are discussed. Different configurations have been considered: sequential or hybrid  
56 reactors, divided or undivided cells, flow-cell or stirred tank reactor and light source  
57 positioning, i.e. external or immersed, vertical or horizontal, on the top or bottom or on the side  
58 of reactor. To obtain maximal synergy and maximum quantum yields, the distance between the  
59 light source and the electrode needs to be minimized. Hybrid reactors in undivided flow-cells  
60 are practically preferred for the lower footprint area, the possibility to regenerate iron catalysts  
61 and the enhancement of mass transfer compared with stirred tank reactor. Moreover, the  
62 interelectrode gap can be easily controlled in flow-cell, which permits optimisation of the

63 penetration depth when the light is applied through the reactor. These insights give some keys  
64 for future development of photo-electrochemical technologies.

65

66 **Keywords** Advanced oxidation • Anodic oxidation • Electrocatalysis • Electro-Fenton •  
67 Photocatalysis • Photo-electrochemical processes • Reactor design • Wastewater

68

69

70  
71  
72  
73  
74  
75  
76  
77  
78  
79  
80  
81  
82  
83  
84  
85  
86  
87  
88  
89  
90  
91

## Contents

1. Introduction .....	5
2. Influence of catalytic oxidation .....	6
2.1. Selection of electrode materials for electrocatalytic oxidation .....	6
2.2. Selection of photocatalyst for photocatalytic oxidation .....	10
2.3. Selection of the catalyst support for electrocatalytic and photocatalytic oxidation combination .....	11
3. Reactor design .....	19
3.1. Sequential versus hybrid reactors .....	23
3.2. Reactor configuration: divided versus undivided cells .....	24
3.3. Operation mode: flow-cell versus stirred tank reactor .....	25
3.4. Light source positioning .....	26
4. Conclusion .....	30
References .....	30

## 92        **1. Introduction**

93        The release of hazardous micropollutants such as pesticides, pharmaceuticals and personal care  
94        products at the outlet of wastewater treatment plants into the water bodies is a problem of major  
95        concern (UNESCO 2017). These contaminants can be potentially toxic for the environment and  
96        human health even at very low concentrations (pg/L to µg/L) (Luo et al. 2014; Cizmas et al.  
97        2015).

98        The biological processes involved in conventional treatment plants are not suitable enough to  
99        remove completely these biorecalcitrant compounds (Besnault and Martin 2011). Therefore,  
100        advanced physical-chemical technologies have been proposed to answer this issue and among  
101        them advanced oxidation processes have gained interest (Shi et al. 2020). They all rely on the  
102        generation of very strong oxidizing agents such as hydroxyl radicals ( $\cdot\text{OH}$ ) having a high  
103        standard potential ( $E^\circ(\cdot\text{OH}/\text{H}_2\text{O})$ ) that is equal to 2.80 V versus the standard hydrogen  
104        electrode, noted in V for the sake of simplicity in all the chapter (Glaze et al. 1987; Oturan and  
105        Aaron 2014; Stefan 2017).  $\cdot\text{OH}$  radical is a reactive oxygen species that has a very short lifetime  
106        in the range of nanoseconds, which avoids its persistence into the environment (Gligorovski et  
107        al. 2015).  $\cdot\text{OH}$  radical is also known for its almost non-selectivity due to its four reaction modes,  
108        i.e. hydrogen atom abstraction, electrophilic addition to unsaturated bonds, electron transfer  
109        and the ipso-substitution with perhalogenocarbon compounds, which permit the oxidation of a  
110        broad spectrum of compounds (Dorfman and Adams 1973; Von Sonntag 2008; Mousset et al.  
111        2018a).  $\cdot\text{OH}$  reaction is particularly fast with C=C double bonds that are present in molecular  
112        structure of many organic micropollutants, with oxidation rate constants ranging from  $10^8$  to  
113         $10^{10} \text{ L mol}^{-1} \text{ s}^{-1}$  (Mousset et al., 2016a).

114        Among advanced oxidation processes there are the traditional chemical ones that involve either  
115        (i) an oxidant such as hydrogen peroxide ( $\text{H}_2\text{O}_2$ ) and a catalyst such as ferrous ion ( $\text{Fe}^{2+}$ ), known  
116        as Fenton or Fenton-like processes, or (ii) photons produced by light irradiation photolysing an  
117        oxidant like  $\text{H}_2\text{O}_2$  (Oturan and Aaron 2014). These processes present some drawbacks such as  
118        the need to continuously add reagents such as  $\text{H}_2\text{O}_2$  (Oturan and Aaron 2014) or have  
119        applicability at a limited pH range. At the end of the nineties, the electrochemical-based  
120        advanced oxidation processes have been proposed as an alternative for producing *in situ* and  
121        continuously the oxidant species during the electrolysis, the electron being the main reagent  
122        involved (Brillas et al. 2009; Panizza and Cerisola 2009; Vasudevan and Oturan 2014; Sirés et  
123        al. 2014; Martínez-Huitle et al. 2015; Moreira et al. 2017). These characteristics make

124 electrochemical advanced oxidation processes gaining great interest in the scientific  
125 community since degradation and mineralisation yields can reached higher than 99% for a wide  
126 range of organic pollutant and organic load represented by a chemical oxygen demand below  
127 100 g-O<sub>2</sub> L<sup>-1</sup> (Lahkimi et al. 2007; Alcántara et al. 2009; Mousset et al. 2013, 2014a, b; Sirés  
128 et al. 2014; dos Santos et al. 2015, 2017; Shukla and Oturan 2015; Ganzenko et al. 2018).  
129 More recently, photo-assisted electrochemical processes have been proposed in order to make  
130 use of renewable energy in response to the sustainable development objectives (Garcia-Segura  
131 et al. 2013; Garza-Campos et al. 2014; Ramirez et al. 2015; Mousset et al. 2017a). Photo-  
132 electrochemical processes have been applied for the treatment of biorefractory pollutants as  
133 reviewed recently (dos Santos and Scialdone 2018). Dyes are presents in textile effluents and  
134 they could be treated for discoloration and mineralisation (Martínez-Huitle and Brillas 2009;  
135 Zhao et al. 2010; Zhou et al. 2010; Xu et al. 2013; Brillas and Martínez-Huitle 2015). Pesticides  
136 released in wastewater (Fang et al. 2012; Almazán-Sánchez et al. 2017) have also been removed  
137 by photo-electrochemical processes. Pharmaceuticals detected as micropollutants in municipal  
138 wastewater treatment plants outflow or in hospital wastewaters could be degraded and  
139 mineralized (Zhao et al. 2009; Feng et al. 2013). Water disinfection is another promising  
140 application of such processes by inactivating pathogenic microorganisms such as bacteria like  
141 *Candida parapsilosis* and *Escherichia coli* (Liu et al. 2014; dos Santos and Scialdone 2018).  
142 Interestingly, synergy in reactions can be obtained in photo-electrochemical combinations,  
143 especially in hybrid reactors. In fact, the reactor design represents an essential engineering  
144 aspects in photoprocesses efficiency. This is the reason why it is proposed to discuss those  
145 facets in the following sections.

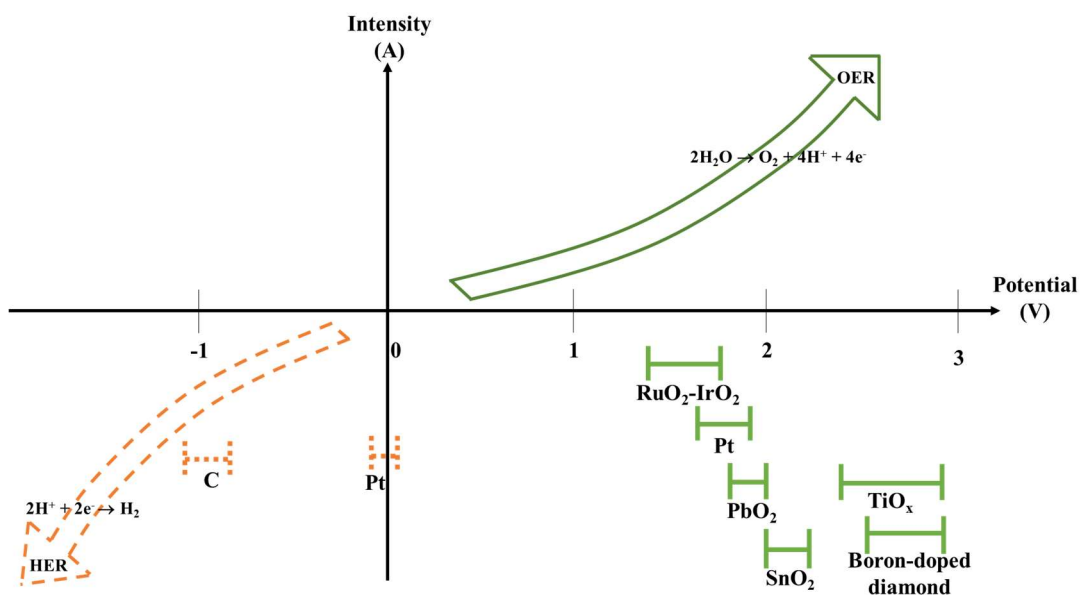
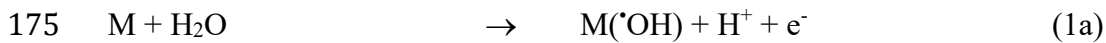
146

## 147 **2. Influence of catalytic oxidation**

### 148 **2.1. Selection of electrode materials for electrocatalytic oxidation**

149 In electrochemical processes, electrode materials play a major role in the removal efficiency  
150 (Mousset et al., 2016c, 2016d; Mousset et al., 2017b; Oturan et al., 2012; Panizza and Martinez-  
151 Huitle, 2013; Yu et al., 2015; Zhou et al., 2014). According to their properties they will act as  
152 catalyst to promote or not the oxidation of organic and inorganic compounds. There are two  
153 ways of oxidation, either by direct electron exchange through redox reactions with electroactive  
154 species, i.e. the so-called direct oxidation, or the indirect oxidation by electrogenerating  
155 oxidizing species at the electrode materials surface (Sirés et al. 2014). The first mode occurs

156 less frequently due to its more specific oxidation behavior, since many organic pollutants are  
 157 not electroactive. The indirect oxidation mode is generally considered as the main degradation  
 158 and mineralisation mechanisms for electrochemical treatment of wastewater. Both anode and  
 159 cathode can play a role in this oxidation process, according to their overvoltage values – also  
 160 known as overpotential values – for oxygen evolution and hydrogen evolution, respectively  
 161 (Figure 1) (Panizza and Cerisola 2009; Comninellis and Chen 2010; Mousset and Zhou 2017).  
 162 The anode materials can be divided into two categories: (i) the active anodes that have a low  
 163 overvoltage for O<sub>2</sub> evolution usually considered below 1.9 V; this is the case of dimensionally  
 164 stable anode (DSA<sup>®</sup>) like RuO<sub>2</sub>-IrO<sub>2</sub> with 1.4-1.7 V and platinum (Pt) in the range of 1.6-1.9  
 165 V, (ii) the non-active anodes that have a high O<sub>2</sub> evolution overvoltage usually considered  
 166 higher than 1.9 V; this is the case of lead dioxide (PbO<sub>2</sub>) with 1.8-2.0 V, tin oxide (SnO<sub>2</sub>) with  
 167 2.0-2.2 V, sub-stoichiometric titanium oxide (Ti<sub>x</sub>O<sub>2x-1</sub> (4 ≤ x ≤ 9)) referred as TiO<sub>x</sub> (x < 2) in  
 168 this chapter (2.4-2.8 V), and boron-doped diamond with 2.2-2.8 V (Panizza and Cerisola 2009;  
 169 Comninellis and Chen 2010). The oxidation involving at active anode materials is referred to  
 170 electro-oxidation in this book chapter. In contrast to the active anodes, high O<sub>2</sub> overvoltage  
 171 materials favor the generation of physisorbed •OH radicals at their surface by water (H<sub>2</sub>O)  
 172 oxidation (Panizza and Cerisola 2009). This weak sorption makes •OH radical available for  
 173 matrix oxidation through the following reactions (Eqs. 1a-1b) at the anode (M) surface material  
 174 (Panizza and Cerisola 2009):

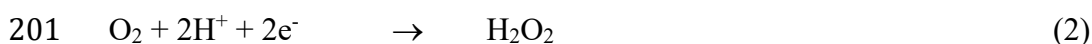


177

178 **Figure 1.** Overvoltage for hydrogen evolution at cathode (dashed line) and oxygen evolution at anode  
179 (full line) materials. OER occurs at the highest potentials using boron-doped diamond and TiO<sub>x</sub>  
180 anodes, which makes them having a high oxidation power. HER occurs at low potential with carbon-  
181 based cathodes, which permit the electro-generation of H<sub>2</sub>O<sub>2</sub> at their surface. Abbreviations: HER:  
182 hydrogen evolution reaction, OER: oxygen evolution reaction.  
183

184 The non-active anodes are preferentially employed due to their benefit that can be obtained  
185 from the •OH production and the subsequent high organic pollutant removal efficiency in an  
186 advanced electro-oxidation technology, that will be referred as anodic oxidation in this chapter.  
187 PbO<sub>2</sub> is a cheap material but has been put aside to avoid the possible release of toxic Pb<sup>2+</sup> ions,  
188 though more recent studies highlight the development of more stable PbO<sub>2</sub>-based anode  
189 (Panizza and Cerisola 2009; Aquino et al. 2014). Boron-doped diamond is the most widely used  
190 anode material in advanced electro-oxidation treatment for its high efficiency and good stability  
191 and resistance (Comminellis and Chen 2010; Brillas and Martinez-Huitle 2011). However, its  
192 relatively high cost makes its application limited to quite small treatment plants. TiO<sub>x</sub> (x < 2)  
193 is gaining interest for its lower cost and its flexibility (Ganiyu et al. 2016, 2017). Though SnO<sub>2</sub>  
194 materials have currently a low stability for wastewater treatment application (Panizza and  
195 Cerisola 2009), its transparency makes it very interesting for hybrid photoelectrochemical  
196 processes (Mousset et al. 2017a) as discussed in sub-section 3.4.

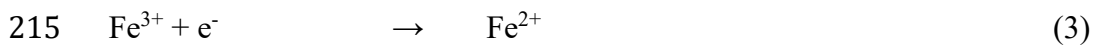
197 The cathode materials can also participate in the oxidation mechanism according to their  
198 hydrogen (H<sub>2</sub>) evolution overvoltage properties (Figure 1). A high H<sub>2</sub> overvoltage can promote  
199 the electrogeneration of hydrogen peroxide (H<sub>2</sub>O<sub>2</sub>) through the two-electron O<sub>2</sub> reduction  
200 reaction (Brillas et al. 2009):



202  
203 Platinum (Pt) is chemically inert in the electrochemical advanced oxidation processes'  
204 operating conditions and is useful for mechanism understanding studies. Though it has been  
205 widely employed at laboratory scale, Pt material is not only expensive but also not efficient to  
206 produce H<sub>2</sub>O<sub>2</sub> (Sopaj 2013). Stainless steel is comparatively a cheap metal material, but the  
207 amount of electrogenerated H<sub>2</sub>O<sub>2</sub> is still very low (Sopaj 2013; Mousset et al. 2018a).

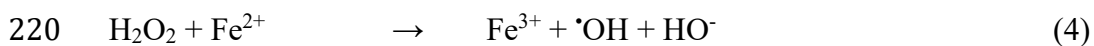
208 Carbon materials have been preferentially studied in the electrochemical advanced oxidation  
209 processes area for their high H<sub>2</sub> overvoltage as well as high stability, high flexibility and low  
210 cost (Brillas et al. 2009; Chaplin 2014). Graphite represents an abundant natural form of carbon

211 and is therefore a cheap carbon material. However, its low specific surface area does not permit  
212 significant level of H<sub>2</sub>O<sub>2</sub> concentration (Mousset et al. 2016d). The three-dimensional structure  
213 of felt form of carbon-based cathode has been widely investigated for its high specific surface  
214 area that allows the fast reduction of Fe<sup>3+</sup> into Fe<sup>2+</sup> (Eq. 3) (Sirés et al. 2007).



216

217 This regeneration reaction permits the continuous production of •OH radicals through Fenton  
218 reaction (Eq. 4) implemented in the so-called homogeneous electro-Fenton process when Fe<sup>2+</sup>  
219 is dissolved or present initially in solution (Brillas et al. 2009; Mousset et al. 2016b):



221

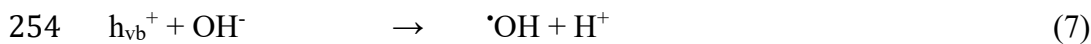
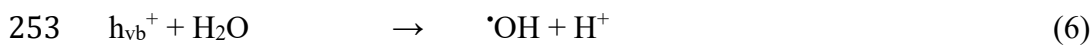
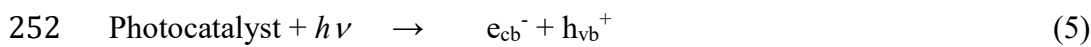
222 Heterogeneous electro-Fenton processes that involve a source of iron, e.g. FeS<sub>2</sub> and Fe<sub>3</sub>O<sub>4</sub>,  
223 coated on the cathode material are emerging (Ganiyu et al. 2018). It avoids the pH adjustment  
224 to 3 unlike in homogeneous Fenton-based technology in which the dissolved Fe<sup>3+</sup> would  
225 precipitate in Fe(OH)<sub>3</sub> otherwise. Sacrificial iron or steel anode materials have been widely  
226 employed as an alternative source of Fe<sup>2+</sup> in peroxi-coagulation process (Brillas et al. 1997,  
227 2003; Ren et al. 2018; Nidheesh 2018). Peroxi-coagulation consists of the combination of  
228 electro-Fenton that electro-generate H<sub>2</sub>O<sub>2</sub> at cathode and electro-coagulation to produce Fe<sup>2+</sup>  
229 by anodic dissolution.

230 Gas diffusion electrodes using carbon-polytetrafluoroethylene have been also suggested as  
231 carbon-based cathode material (Brillas et al. 2009). The O<sub>2</sub> flows through the thin and the  
232 porous carbon material, which enhances the O<sub>2</sub> transfer towards the cathode and therefore the  
233 yield of H<sub>2</sub>O<sub>2</sub> electrogeneration (Sirés et al. 2007; Brillas et al. 2009; Martínez-Huitle et al.  
234 2015). One drawback of gas diffusion electrodes cathodes is their low specific surface area that  
235 limits the rate of Fe<sup>2+</sup> regeneration as compared to three dimensional carbon-based materials  
236 (Sirés et al. 2007). Some efforts have been made to enhance the specific surface area of carbon  
237 materials, including thermal treatment (Le et al. 2016), chemical treatment (Zhou et al. 2014)  
238 and graphene-doped modifications (Garcia-Rodriguez et al., 2018; Le et al., 2015a, 2015b;  
239 Mousset et al., 2017b, 2016c), with encouraging results for both H<sub>2</sub>O<sub>2</sub> electrogeneration and  
240 Fe<sup>2+</sup> regeneration.

241

## 2.2. Selection of photocatalyst for photocatalytic oxidation

Photocatalysis has been widely developed the last few decades as an alternative to traditional chemical advanced oxidation processes, by benefitting from the light to produce strong oxidizing agents like  $\cdot\text{OH}$  radicals using a catalyst (Fujishima et al. 2000; Malato et al. 2009; Lazar et al. 2012; Pelaez et al. 2012; Schneider et al. 2014). This photocatalyst is a semiconductor that possess an energy gap region known as bandgap. Photocatalyst excitation with energy higher (i.e., light irradiation at a specific wavelength) than the bandgap promotes an excited electron into the conduction band ( $e_{cb}^-$ ) leaving behind a positive vacancy namely as a hole ( $h_{vb}^+$ ) (Eq. 5) that can then oxidize water ( $\text{H}_2\text{O}$ ) (Eq. 6) or hydroxide ion ( $\text{OH}^-$ ) (Eq. 7) to produce  $\cdot\text{OH}$  radicals.



255

Among the numerous photocatalysts that have been tested in literature, titanium dioxide ( $\text{TiO}_2$ ) is the most common material employed. The band gap for its anatase crystal phase is 3.2 eV, meaning that ultraviolet - noted UV in this chapter - radiation bellow 387 nm is required to initiate photocatalysis process. These UV-based photocatalysis are energy-consuming processes. Thus, numerous efforts have been devoted to benefit from the use of free solar light that is composed of 40% of visible light, in wavelength ranging from 400 nm to 800 nm. In this context, several visible light active photocatalysts have been proposed in literature with reduced band gap, including modified  $\text{TiO}_2$  (Pelaez et al. 2012; Ding et al. 2012, 2014; Andersen et al. 2014; Barndök et al. 2016; Fagan et al. 2016).

The photocatalysis can be implemented through two ways, either the photocatalyst is in suspension in the effluent to be treated or it is immobilized on a substrate. The first version allows for a higher surface of contact between the catalyst and the photons per unit volume, which can increase the quantum yield (Stefan 2017). However, a further separation stage is required in the treatment since the catalyst has to be recovered before the release of treated wastewater. Therefore, a preliminary catalyst immobilisation step is alternatively considered (Stefan 2017). The catalyst support is then another parameter to take into account for a good coating stability. A further advantage is that conductive substrate could bring synergy when combining electrochemical treatment with heterogeneous photocatalysis as discussed in section 2.3.

275

276 **2.3. Selection of the catalyst support for electrocatalytic and photocatalytic**  
277 **oxidation combination**

278 According to the following criteria, different processes can be implemented or not, i.e.  
279 electrochemical treatments or not, and/or photochemical processes or not, and/or photo-  
280 electrochemical combinations (Table 1):

- 281 (1) presence or not of electrode, involvement or not of high overvoltage electrode
- 282 (2) presence of light or not, presence of photocatalyst or not, presence of photocatalyst
- 283 on electrode or not

284 **Table 1.** Implementation of electrolysis, photochemical processes and possible combinations between  
285 electrolysis and photochemistry, depending on criteria involved. According to the kind of  
286 combination, the processes implemented can vary from a simple photolysis or electro-oxidation to a  
287 more complex system combining electrochemical advanced oxidation processes with  
288 photoelectrocatalysis.  
289

	Absence of light	Light without catalyst	Light with photocatalyst not coated on electrode	Light with photocatalyst coated on electrode
Absence of electrode	∅	Photolysis	Photocatalysis	∅
Absence of high overvoltage electrode	Electro-oxidation	Electro-oxidation/ photolysis	Electro-oxidation/ photocatalysis	Photoelectrocatalysis
High overvoltage electrode	Electro-chemical advanced oxidation processes	Electrochemical advanced oxidation processes/ photolysis	Electrochemical advanced oxidation processes/ photocatalysis	Electrochemical advanced oxidation processes/ photoelectrocatalysis

290  
291 The possible combinations highlight a possible increase of electrocatalytic activity  
292 accompanying by a possible increase of photocatalytic activity according to the criteria  
293 involved. The increase of catalytic activity leads to higher number of •OH production sites as it  
294 has been previously proposed in literature (Brillas et al., 2009; Goldstein et al., 2007; Luo et  
295 al., 2015; Mousset et al., 2017a; Sun and Pignatello, 1993), which is summarized in Table 2  
296 and displayed in Figure 2.

297 As represented in Table 2 and Figure 2, the electro-oxidation process does not bring any source  
298 of •OH production, since only direct oxidation occurs. When electro-oxidation is combined to

299 photolysis (electro-oxidation/photolysis), there is no  $\cdot\text{OH}$  production as well, since only  
300 photosensitive pollutants are degraded by photolysis. In electro-oxidation/photocatalysis the  
301  $\cdot\text{OH}$  production site is coming from the photocatalysis itself as explained in sub-section 2.2.  
302 Similarly, photoelectrocatalysis lead to the generation of one  $\cdot\text{OH}$  site. Still, a difference of  
303 oxidation efficiency can be observed between photocatalysis and photoelectrocatalysis  
304 processes. An important waste reaction occurs during the photocatalysis mechanism, which  
305 consists on the electron/hole pair recombination (Eq. 8) (Schneider et al. 2014):

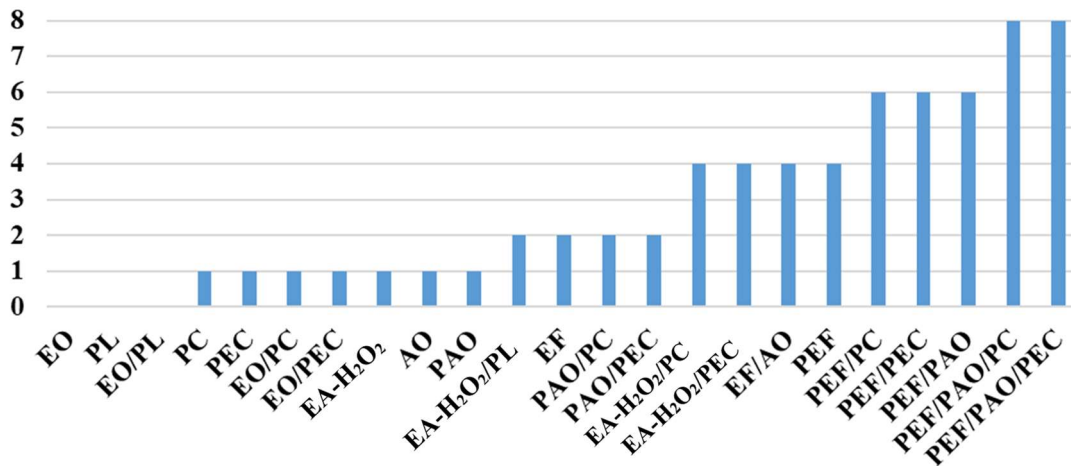


307

308  
309 **Table 2.** Number of  $\cdot\text{OH}$  production sites according to the kind of combination between electrolysis  
310 and photochemical processes. There is no  $\cdot\text{OH}$  production in electro-oxidation system combined with  
311 photolysis. Implementing photocatalysis or photoelectrocatalysis results in increasing the number of  
312  $\cdot\text{OH}$  production site by one. The number of  $\cdot\text{OH}$  production site drastically increases when  
313 electrochemical advanced oxidation processes such as anodic oxidation and/or electro-Fenton are  
314 involved. Their combination with photolysis or photocatalysis/photoelectrocatalysis increases even  
315 higher the number of  $\cdot\text{OH}$  production site due to synergy. Abbreviations: AO: anodic oxidation, EA-  
316  $\text{H}_2\text{O}_2$ :  $\text{H}_2\text{O}_2$  electro-activation, EO: electro-oxidation,  $\text{H}_2\text{O}_2\text{-O}_2^{\cdot-}$ :  $\text{H}_2\text{O}_2$  reaction with  $\text{O}_2^{\cdot-}$ , PL:  
317 photolysis, PC: photocatalysis, PEC: photoelectrocatalysis.

Electrochemical process	Photochemical process		
	Photolysis (0 × $\cdot\text{OH}$ )	Photocatalysis (1 × $\cdot\text{OH}$ )	Photoelectrocatalysis (1 × $\cdot\text{OH}$ )
<b>Electro-oxidation</b> (0 × $\cdot\text{OH}$ )	$(0 \times \cdot\text{OH})_{\text{PL}}$ + $(0 \times \cdot\text{OH})_{\text{EO}}$ <b>= 0 × <math>\cdot\text{OH}</math></b>	$(1 \times \cdot\text{OH})_{\text{PC}}$ + $(0 \times \cdot\text{OH})_{\text{EO}}$ <b>= 1 × <math>\cdot\text{OH}</math></b>	$(1 \times \cdot\text{OH})_{\text{PC}}$ + $(0 \times \cdot\text{OH})_{\text{EO}}$ <b>= 1 × <math>\cdot\text{OH}</math></b>
<b><math>\text{H}_2\text{O}_2</math> electro-activation</b> (1 × $\cdot\text{OH}$ )	$(0 \times \cdot\text{OH})_{\text{PL}}$ + $(1 \times \cdot\text{OH})_{\text{EA-H}_2\text{O}_2}$ + $(1 \times \cdot\text{OH})_{\text{synergyPL/EA-H}_2\text{O}_2}$ <b>= 2 × <math>\cdot\text{OH}</math></b>	$(1 \times \cdot\text{OH})_{\text{PC}}$ + $(1 \times \cdot\text{OH})_{\text{EA-H}_2\text{O}_2}$ + $(1 \times \cdot\text{OH})_{\text{synergyPL/EA-H}_2\text{O}_2}$ + $(1 \times \cdot\text{OH})_{\text{H}_2\text{O}_2\text{-O}_2^{\cdot-}}$ <b>= 4 × <math>\cdot\text{OH}</math></b>	$(1 \times \cdot\text{OH})_{\text{PC}}$ + $(1 \times \cdot\text{OH})_{\text{EA-H}_2\text{O}_2}$ + $(1 \times \cdot\text{OH})_{\text{synergyPL/EA-H}_2\text{O}_2}$ + $(1 \times \cdot\text{OH})_{\text{H}_2\text{O}_2\text{-O}_2^{\cdot-}}$ <b>= 4 × <math>\cdot\text{OH}</math></b>
<b>Anodic oxidation</b> (1 × $\cdot\text{OH}$ )	$(0 \times \cdot\text{OH})_{\text{PL}}$ + $(1 \times \cdot\text{OH})_{\text{AO}}$ <b>= 1 × <math>\cdot\text{OH}</math></b>	$(1 \times \cdot\text{OH})_{\text{PC}}$ + $(1 \times \cdot\text{OH})_{\text{AO}}$ <b>= 2 × <math>\cdot\text{OH}</math></b>	$(1 \times \cdot\text{OH})_{\text{PC}}$ + $(1 \times \cdot\text{OH})_{\text{AO}}$ <b>= 2 × <math>\cdot\text{OH}</math></b>
<b>Electro-Fenton</b> (2 × $\cdot\text{OH}$ )	$(0 \times \cdot\text{OH})_{\text{PL}}$ + $(1 \times \cdot\text{OH})_{\text{EF}}$ + $(1 \times \cdot\text{OH})_{\text{EA-H}_2\text{O}_2}$ + $(1 \times \cdot\text{OH})_{\text{synergyPL/EA-H}_2\text{O}_2}$ + $(1 \times \cdot\text{OH})_{\text{synergyPL/EF}}$ <b>= 4 × <math>\cdot\text{OH}</math></b>	$(1 \times \cdot\text{OH})_{\text{PC}}$ + $(1 \times \cdot\text{OH})_{\text{EF}}$ + $(1 \times \cdot\text{OH})_{\text{EA-H}_2\text{O}_2}$ + $(1 \times \cdot\text{OH})_{\text{synergyPL/EA-H}_2\text{O}_2}$ + $(1 \times \cdot\text{OH})_{\text{synergyPL/EF}}$ + $(1 \times \cdot\text{OH})_{\text{H}_2\text{O}_2\text{-O}_2^{\cdot-}}$ <b>= 6 × <math>\cdot\text{OH}</math></b>	$(1 \times \cdot\text{OH})_{\text{PC}}$ + $(1 \times \cdot\text{OH})_{\text{EF}}$ + $(1 \times \cdot\text{OH})_{\text{EA-H}_2\text{O}_2}$ + $(1 \times \cdot\text{OH})_{\text{synergyPL/EA-H}_2\text{O}_2}$ + $(1 \times \cdot\text{OH})_{\text{synergyPL/EF}}$ + $(1 \times \cdot\text{OH})_{\text{H}_2\text{O}_2\text{-O}_2^{\cdot-}}$ <b>= 6 × <math>\cdot\text{OH}</math></b>
<b>Electro-Fenton/anodic oxidation</b> (4 × $\cdot\text{OH}$ )	$(0 \times \cdot\text{OH})_{\text{PL}}$ + $(1 \times \cdot\text{OH})_{\text{EF}}$ + $(1 \times \cdot\text{OH})_{\text{AO}}$ + $(1 \times \cdot\text{OH})_{\text{EA-H}_2\text{O}_2}$ + $(1 \times \cdot\text{OH})_{\text{synergyEF/AO-peroxone}}$ + $(1 \times \cdot\text{OH})_{\text{synergyPL/EA-H}_2\text{O}_2}$ + $(1 \times \cdot\text{OH})_{\text{synergyPL/EF}}$ <b>= 6 × <math>\cdot\text{OH}</math></b>	$(1 \times \cdot\text{OH})_{\text{PC}}$ + $(1 \times \cdot\text{OH})_{\text{EF}}$ + $(1 \times \cdot\text{OH})_{\text{AO}}$ + $(1 \times \cdot\text{OH})_{\text{EA-H}_2\text{O}_2}$ + $(1 \times \cdot\text{OH})_{\text{synergyEF/AO-peroxone}}$ + $(1 \times \cdot\text{OH})_{\text{synergyPL/EA-H}_2\text{O}_2}$ + $(1 \times \cdot\text{OH})_{\text{synergyPL/EF}}$ + $(1 \times \cdot\text{OH})_{\text{H}_2\text{O}_2\text{-O}_2^{\cdot-}}$ <b>= 8 × <math>\cdot\text{OH}</math></b>	$(1 \times \cdot\text{OH})_{\text{PC}}$ + $(1 \times \cdot\text{OH})_{\text{EF}}$ + $(1 \times \cdot\text{OH})_{\text{AO}}$ + $(1 \times \cdot\text{OH})_{\text{EA-H}_2\text{O}_2}$ + $(1 \times \cdot\text{OH})_{\text{synergyPL/EA-H}_2\text{O}_2}$ + $(1 \times \cdot\text{OH})_{\text{synergyPL/EF}}$ + $(1 \times \cdot\text{OH})_{\text{synergyEF/AO-peroxone}}$ + $(1 \times \cdot\text{OH})_{\text{H}_2\text{O}_2\text{-O}_2^{\cdot-}}$ <b>= 8 × <math>\cdot\text{OH}</math></b>

**Number of  $\cdot\text{OH}$   
active sites**



319

320 **Figure 2.** Number of  $\cdot\text{OH}$  active sites according to the single and combined processes implemented.

321 The combination giving the maximum number of  $\cdot\text{OH}$  production site, i.e. eight production sites, is  
322 photoelectro-Fenton with photoanodic oxidation and photocatalysis or photoelectrocatalysis.

323 Abbreviations: AO: anodic oxidation, EA-H<sub>2</sub>O<sub>2</sub>: H<sub>2</sub>O<sub>2</sub> electro-activation, EO: electro-oxidation, PAO:

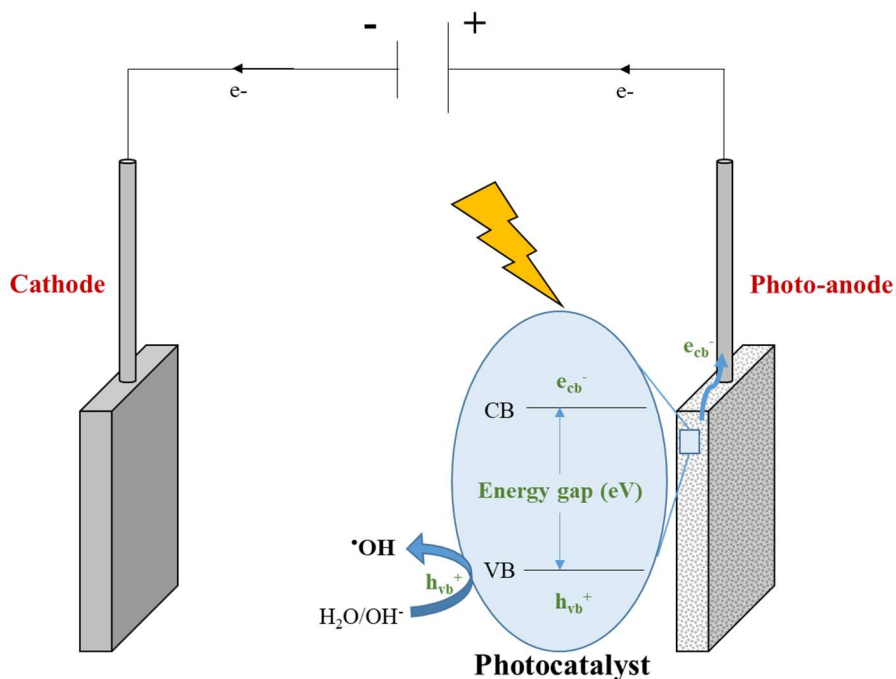
324 photoanodic oxidation, PC: photocatalysis, PEC: photoelectrocatalysis, PEF: photoelectro-Fenton, PL:

325 photolysis.

326

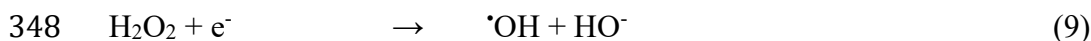
327 In photoelectrocatalysis, the photocatalyst is coated on a conductive material that can be used  
328 as an electrode in the electrolysis process (Catanho et al. 2006; Esquivel et al. 2009; Liu et al.  
329 2009; Ding et al. 2012; Daskalaki et al. 2013; Garcia-Segura et al. 2013; Zhai et al. 2013;  
330 Ramirez et al. 2015; Bessegato et al. 2015). This configuration has the advantage to reduce the  
331 charge recombination (Zhai et al. 2013; Bessegato et al. 2015), as depicted in Figure 3. This  
332 enhances the degradation and mineralisation efficiency as demonstrated previously by Ding et  
333 al. (2012) who noticed a 2.5 times increase of degradation rate with photoelectrocatalysis-based  
334 process as compared to photocatalysis technology. This synergistic effect can be ascribed to the  
335 transfer of photo-electrons to the cathode that enhance the electro-generation of H<sub>2</sub>O<sub>2</sub> for  
336 electro-Fenton process while limiting the charge recombination in photocatalysis mechanism  
337 (Ding et al. 2012).

338



339  
 340 **Figure 3.** Photoelectrocatalysis process combining the electrolysis with a photo-anode. The advantage  
 341 of this system compared to photocatalysis is that it limits the charge recombination, i.e.  $e_{cb}^-$  and  $h_{vb}^+$ ,  
 342 since the electron ( $e_{cb}^-$ ) is driven to the cathode. Abbreviations: CB: conductive band,  $e_{cb}^-$ : electron in  
 343 the conduction band,  $h_{vb}^+$ : positive vacancy (hole) in the valence band, VB: valence band.

344  
 345 In the presence of the cathodic generation of  $H_2O_2$ , it has recently been demonstrated that  $\cdot OH$   
 346 radicals could be formed through electro-activation of  $H_2O_2$  with one electron (Eq. 9) (Luo et  
 347 al. 2015):

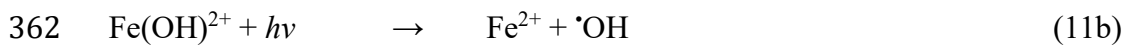


349  
 350 When  $H_2O_2$  electro-activation is combined with photocatalysis or photoelectrocatalysis, a  
 351 synergy could be observed with the  $H_2O_2$  photolysis under UVC irradiation ( $\lambda < 280$  nm) by  
 352 homolytic cleavage giving another source of  $\cdot OH$  (Eq. 10) (Goldstein et al. 2007):



354  
 355 Anodic oxidation process combined with photolysis – referred as photoanodic oxidation in this  
 356 chapter – cannot bring another production site of  $\cdot OH$  (Table 2). Interestingly, electro-Fenton  
 357 can bring synergy in electro-Fenton/photolysis combination, namely photoelectro-Fenton  
 358 process, through the UV irradiation of Fe(III)-monohydroxy complex ( $Fe(OH)^{2+}$ ) that

359 represents an additional  $\cdot\text{OH}$  production source (Eqs. 11a-11b) (Sun and Pignatello 1993;  
360 Brillas et al. 2009):

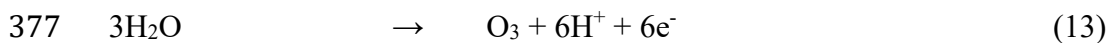
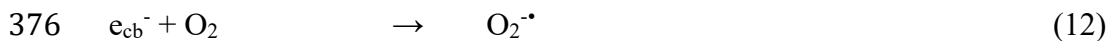


363

364  $\text{Fe}(\text{OH})^{2+}$  is the predominant Fe(III) species at pH around 3 (Faust and Hoigné 1990), which  
365 corresponds to the optimal pH for electro-Fenton process (Brillas et al. 2009; Mousset et al.  
366 2016e). Therefore, the production rate of  $\text{Fe}(\text{OH})^{2+}$  is not negligible and indirectly the  $\cdot\text{OH}$   
367 production as well. In addition, the UV light allow the regeneration of  $\text{Fe}^{2+}$  in the meanwhile  
368 from Eq. 11b.

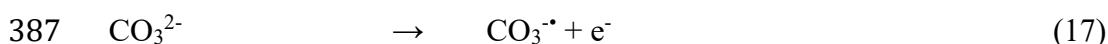
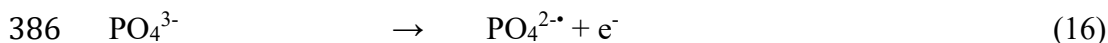
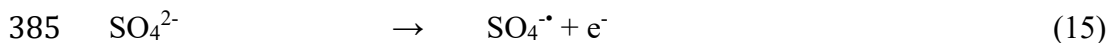
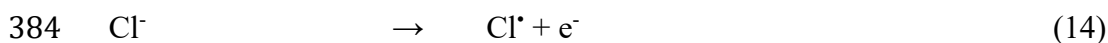
369

370 It is critical to underline that  $\cdot\text{OH}$  is not the sole oxidant that can participate in the organic  
371 removal efficiency. Mediated oxidation can also occur during the photoelectrochemical  
372 processes, by the production of weaker oxidants such as some reactive oxygen species like  
373 superoxide anion ( $\text{O}_2^{\cdot-}$ ) (Eq. 12) in photocatalysis and photoelectrocatalysis processes and  
374 ozone ( $\text{O}_3$ ) (Eq. 13) with non-active anodes in anodic oxidation technology (Bergmann et al.  
375 2009; dos Santos and Scialdone 2018):



378

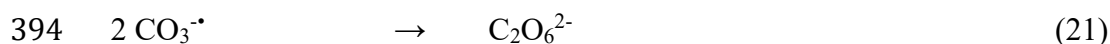
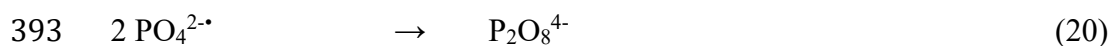
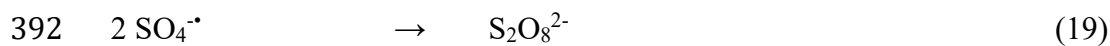
379 Furthermore, depending on the characteristic of the effluent to treat and/or on the supporting  
380 electrolyte that is potentially added, the presence of chloride ion ( $\text{Cl}^-$ ), sulfate ion ( $\text{SO}_4^{2-}$ ),  
381 phosphate ion ( $\text{PO}_4^{3-}$ ), and carbonate ion ( $\text{CO}_3^{2-}$ ) can lead to the formation of radical species  
382 such as  $\text{Cl}^\cdot$  (Eq. 14),  $\text{SO}_4^{\cdot-}$  (Eq. 15),  $\text{PO}_4^{2\cdot-}$  (Eq. 16),  $\text{CO}_3^{\cdot-}$  (Eq. 17), respectively (Sirés et al.  
383 2014):



388

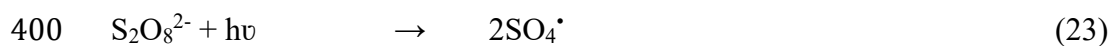
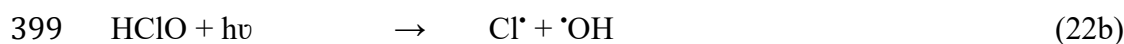
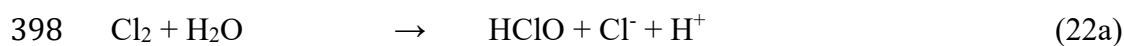
389 More stable oxidants can be generated from these radical species ( $\text{Cl}_2$  (Eq. 18),  $\text{S}_2\text{O}_8^{2-}$  (Eq. 19),  
390  $\text{P}_2\text{O}_8^{4-}$  (Eq. 20),  $\text{C}_2\text{O}_6^{2-}$  (Eq. 21)) (Moreira et al. 2017):





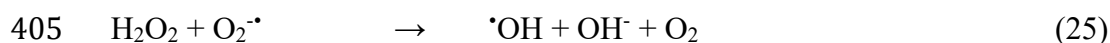
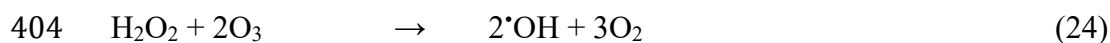
395

396 Under light irradiation,  $\text{Cl}_2$  and  $\text{S}_2\text{O}_8^{2-}$  can generate  $\text{Cl}^{\cdot}$  (Eqs. 22a-22b) and  $\text{SO}_4^{\cdot-}$  (Eq. 23),  
 397 respectively (dos Santos and Scialdone 2018):



401

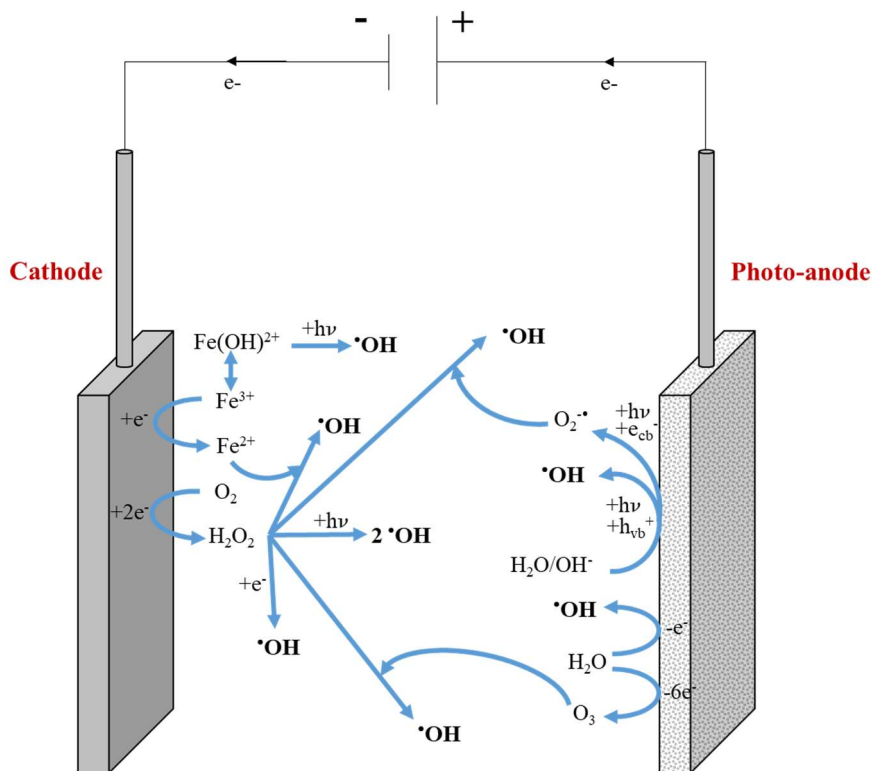
402 This mediated oxidation can also lead to additional production source of  $\cdot\text{OH}$  through peroxone  
 403 equation (Eq. 24) and  $\text{H}_2\text{O}_2$  reaction with  $\text{O}_2^{\cdot-}$  (Eq. 25) (Brillas et al. 2009; Merényi et al. 2010):



406

407 However, mediated oxidants such as chlorinated ones can lead to toxic inorganic, e.g. chlorate  
 408 ( $\text{ClO}_3^-$ ) and perchlorate ( $\text{ClO}_4^-$ ), and organic intermediates such as trihalomethanes (THMs) and  
 409 chloroform that accumulate in solution (Araújo et al. 2015; Brito et al. 2015; Mousset et al.  
 410 2018b, 2020). It is therefore important to control their concentration and to adapt the operating  
 411 conditions in order to limit their formation.

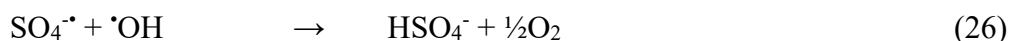
412 Interestingly, the combination that could give theoretically the highest number of  $\cdot\text{OH}$   
 413 production sites, i.e. 8 production sites, is photoelectro-Fenton with photoanodic oxidation and  
 414 photocatalysis or photoelectrocatalysis, i.e. photoelectro-Fenton/photoanodic  
 415 oxidation/photocatalysis or photoelectro-Fenton/photoanodic oxidation/photoelectrocatalysis  
 416 respectively (Mousset et al. 2017a), as schematically presented in Figure 4.

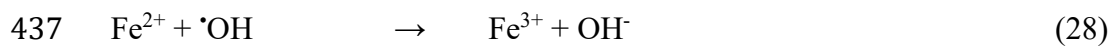


417  
 418 **Figure 4.** Different  $\cdot\text{OH}$  production sites in the photoelectro-Fenton/photoanodic  
 419 oxidation/photoelectrocatalysis process combining electrochemical advanced oxidation processes with  
 420 photoelectrocatalysis. There is a maximum of eight  $\cdot\text{OH}$  production sites from eight different reactions  
 421 involved at the photo-anode, at the cathode and in the bulk solution. It is important to highlight that  
 422 the occurrence of these reactions is depending on the solution pH, the applied wavelength, and the  
 423 production rate of reagent such as  $\text{H}_2\text{O}_2$  involved in parallel reactions.

424  
 425 It is important to emphasize the fact that a higher number of  $\cdot\text{OH}$  production sites does not  
 426 systematically mean that the oxidation efficiency will be better. There can be kinetic  
 427 competitions with reactions requiring the same reagents to produce  $\cdot\text{OH}$  radicals. For instance,  
 428  $\text{H}_2\text{O}_2$  is involved in Fenton reaction (Eq. 4) but also in  $\text{H}_2\text{O}_2$  electro-activation (Eq. 9), in  $\text{H}_2\text{O}_2$   
 429 photolysis (Eq. 10), in peroxone equation (Eq. 24) and in reaction with  $\text{O}_2\cdot^-$  (Eq. 25), meaning  
 430 that the  $\cdot\text{OH}$  production yield will not be automatically increased through five production sites  
 431 instead of one at constant electrogeneration of  $\text{H}_2\text{O}_2$ , the rate of  $\text{H}_2\text{O}_2$  production being the  
 432 limiting step (Mousset et al. 2017a).

433 Moreover, some side reactions that consume  $\cdot\text{OH}$  can limit its action (dos Santos and Scialdone  
 434 2018):





438

439 The reaction between  $\text{Fe}^{2+}$  and  $\cdot\text{OH}$  (Eq. 28) is particularly an important parasitic reactions in  
440 Fenton-based processes (Brillas et al. 2009; Mousset et al. 2016a). In addition, the solution pH  
441 can interfere in the number of  $\cdot\text{OH}$  production sites since the Fenton reaction is optimal at pH  
442 3 in homogeneous systems (Brillas et al. 2009). In contrast,  $\text{O}_2^{\cdot-}$  species is predominant at pH  
443 higher than 6.8, considering a pKa ( $\text{HO}_2^{\cdot}/\text{O}_2^{\cdot-}$ ) equal to 4.8, and therefore the generation of  $\cdot\text{OH}$   
444 through Eq. 25 is optimal at circumneutral pH (Mousset et al. 2018a). Implementing  
445 heterogeneous electro-Fenton process in combination to photoelectrocatalysis could solve this  
446 issue. The wavelength range of light irradiation also plays a role in the number of  $\cdot\text{OH}$   
447 production sites. Thus,  $\text{H}_2\text{O}_2$  photolysis mainly occurs under UVC irradiation ( $\lambda < 280$  nm),  
448 while photocatalysis and photoelectrocatalysis are often performed using UVA ( $315$  nm  $< \lambda <$   
449  $400$  nm) and even visible light irradiation ( $400$  nm  $< \lambda < 800$  nm). It should be emphasized that  
450 the synergy of combinations between  $\text{H}_2\text{O}_2$  photolysis and photocatalysis or  
451 photoelectrocatalysis, i.e. in  $\text{H}_2\text{O}_2$  electro-activation/photocatalysis,  $\text{H}_2\text{O}_2$  electro-  
452 activation/photoelectrocatalysis, photoelectro-Fenton/photocatalysis, photoelectro-  
453 Fenton/photoelectrocatalysis, photoelectro-Fenton/photoanodic oxidation/photocatalysis,  
454 photoelectro-Fenton/photoanodic oxidation/photoelectrocatalysis, cannot occur if the  
455 photocatalyst does not absorb light under UVC irradiation and/or for economic reason if the  
456 system is operated under solar light. The organic load has an impact on the kinetics of  
457 degradation rates but should not hamper the number of  $\cdot\text{OH}$  production sites (Garcia-Segura et  
458 al. 2014). This is the case only if the turbidity is not impacted by the increase of organic load,  
459 otherwise the yields of UV-based reactions will be altered.

460

461

462 The combination of processes along with possible synergy can be optimized via reactor design  
463 that need to be adapted according to the reactions involved as discussed in section 3.

464

### 465 **3. Reactor design**

466 The reactor design is an important parameter to take into account in order to optimize the photo-  
467 electrochemical technologies. The existing combinations between electrolysis and

468 photocatalysis or photoelectrocatalysis technologies proposed in literature for wastewater  
469 treatment application are presented in Table 3. The influence of criteria studied in literature  
470 about the photo-electrochemical reactor design is presented in the following sub-sections 3.2,  
471 3.3 and 3.4.

472

**Table 3.** Processes combination between electrolysis and photocatalysis or photoelectrocatalysis processes proposed in literature for wastewater treatment application. Different reactor designs have been proposed: sequential or hybrid reactors, divided or undivided cells, flow-cell or stirred tank reactor, external or immersed light source, light source positioned on the top or bottom or on the side of reactor, light source placed vertically or horizontally.

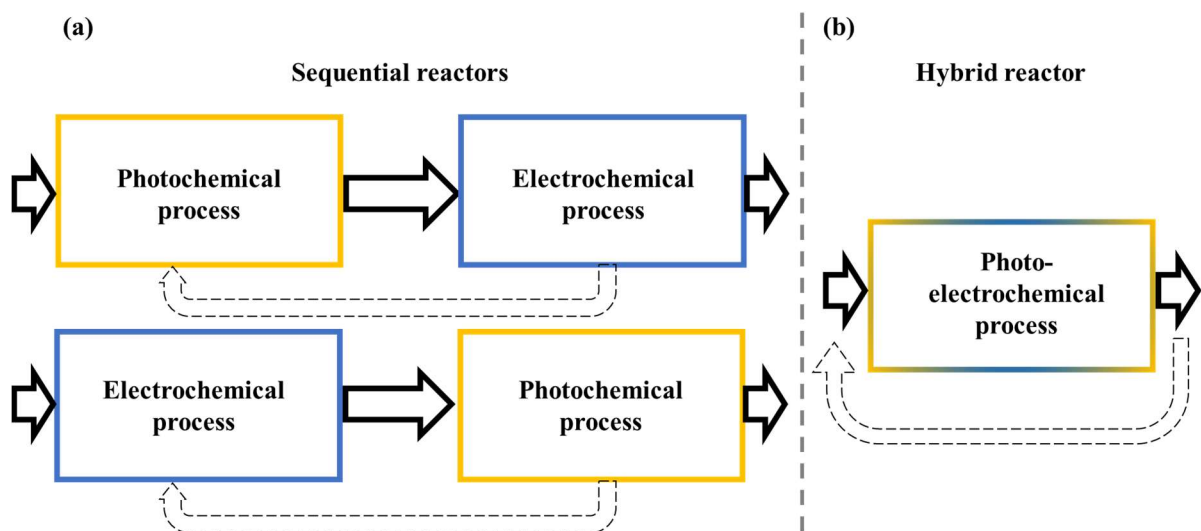
Processes implemented	Reactor configuration	Cathode	Anode	Electrode positioning	Photocatalyst	Kind of light	Light source positioning	Reference
Photoelectro-Fenton/photocatalysis	Undivided cell Cylindrical stirred tank photo-reactor	Boron-doped diamond	Boron-doped diamond	Both parallel and vertical	TiO <sub>2</sub> immobilized on glass spheres and horizontal nylon mesh	Solar light	Externally, on the top of the reactor	(Garza-Campos et al. 2014)
Photoelectro-Fenton/photocatalysis	Undivided cell Electrochemical flow-cell Sequential reactors (electrolyser→photoreactors) in recirculation	Carbon-polytetrafluoroethylene air diffusion cathode	Pt	Both parallel and vertical	TiO <sub>2</sub> immobilized on glass spheres	Solar light	Externally, on the top of the reactor	(Garza-Campos et al. 2016)
Photoelectro-Fenton/photocatalysis	Undivided cell Parallelepiped stirred tank photo-reactor	Graphite/Carbon nanotubes	Pt	Both parallel and vertical	TiO <sub>2</sub> immobilized on glass plates on vertical sides of the reactor	UV light	Immersed vertically in the reactor	(Khataee et al. 2012)
Photoelectro-Fenton/photoanodic oxidation/photocatalysis	Undivided cell Cylindrical glass stirred tank photo-reactor	Carbon felt	Glass/fluorine-doped tin oxide (transparent)	Both parallel and vertical	TiO <sub>2</sub> immobilized on cylindrical glass reactor	UV light	Externally, on the side of the reactor, close to the cathode	(Mousset et al. 2017a)
Photoelectrocatalysis	Undivided cell Cylindrical stirred tank photo-reactor	Ti/Ru	Boron-doped TiO <sub>2</sub> nanotubes	Both parallel and vertical	TiO <sub>2</sub>	UV/Visible light	Immersed vertically in the reactor	(Bessegato et al. 2015)
Photoelectrocatalysis	Undivided cell Cylindrical quartz stirred tank photo-reactor	Pt	Carbon cloth/reduced graphene oxide/TiO <sub>2</sub>	Both parallel and vertical	TiO <sub>2</sub>	Visible light	Not specified	(Zhai et al. 2013)
Photoelectrocatalysis	Undivided cell Cylindrical stirred tank photo-reactor	Boron-doped diamond	Indium tin oxide/TiO <sub>2</sub>	Anode: horizontal	TiO <sub>2</sub>	Solar light	Externally, on the top of the reactor	(Daskalaki et al. 2013)

				(at the bottom) Cathode: vertical				
Photoelectrocatalysis	Undivided cell Cylindrical stirred tank photo-reactor	Carbon-polytetrafluoroethylene air diffusion cathode	Stainless steel/TiO <sub>2</sub>	Anode: oblique Cathode: vertical	TiO <sub>2</sub>	Solar light	Externally, on the top of the reactor	(Garcia-Segura et al. 2013)
Photoelectrocatalysis	Undivided cell Photo-electrochemical flow-cell	Ti mesh on a quartz plate (transparent)	Ti/Ru <sub>0.3</sub> Ti <sub>0.7</sub> O <sub>2</sub>	Both parallel and vertical	Ti <sub>0.7</sub> O <sub>2</sub>	UV light	Externally, on the side of the reactor, close to the cathode	(Catanho et al. 2006)
Photoelectro-Fenton/ photoelectrocatalysis	Undivided cell Cylindrical quartz stirred tank photo-reactor	Reticulated vitreous carbon	Ti/TiO <sub>2</sub>	Anode: horizontal (at the bottom) Cathode: vertical	TiO <sub>2</sub>	UV/Visible light	Externally, at the bottom of the reactor	(Xie and Li 2006)
Photoelectro-Fenton/ photoelectrocatalysis	Divided cell Cylindrical quartz stirred tank photo-reactors	Carbon felt	Ti/TiO <sub>2</sub>	Both parallel and vertical	TiO <sub>2</sub>	UV light	Externally, on the side of the anodic compartment	(Ramirez et al. 2015)
Photoelectro-Fenton/ photoelectrocatalysis	Divided cell Cylindrical glass stirred tank photo-reactor	Carbon cloth	Antimony-doped tin oxide/Optical fibre/TiO <sub>2</sub> (transparent)	Both parallel and vertical	TiO <sub>2</sub>	UV light	Immersed vertically in the reactor	(Esquivel et al. 2009)
Photoelectro-Fenton/photoanodic oxidation/ photoelectrocatalysis	Undivided cell semi-cylindrical quartz stirred tank photo-reactor	Activated carbon fibre/Fe@Fe <sub>2</sub> O <sub>3</sub>	Glass/fluorine-doped tin oxide/Bi <sub>2</sub> WO <sub>6</sub> (transparent)	Both parallel and vertical; anode close to the flat side of the reactor	Bi <sub>2</sub> WO <sub>6</sub> (visible light active)	Visible light	Externally, on the flat side of the reactor	(Ding et al. 2012)

453

### 454 3.1. Sequential versus hybrid reactors

455 There are two possibilities to consider the combination between photochemical and  
456 electrochemical processes combination. The first one is a configuration as sequential reactors  
457 with a possibility of recirculation of the effluent (Figure 5a). The photochemical process can be  
458 either positioned as primary treatment followed by the electrochemical process or in the reverse  
459 order. If a continuous system is considered without recirculation, the electrochemical  
460 technology has advantages to be placed first because the stable oxidizing species such as  $H_2O_2$   
461 formed by the electrode materials can then be photolysed in the photo process and produce  $\cdot OH$   
462 radicals (Garcia-Segura and Brillas 2014; Garza-Campos et al. 2016). In the same way, the  
463 ferro-hydroxy complex formed in the electrolyser can also be photolysed in the subsequent  
464 photo-reactor (Garcia-Segura and Brillas 2014; Garza-Campos et al. 2016).  
465



466

467 **Figure 5.** Sequential (a) versus hybrid (b) reactors for photochemical and electrochemical processes  
468 combination. In a continuous system an electrochemical process followed by a photochemical  
469 technology has the advantage to produce  $\cdot OH$  from the photolysis of some species such as  $H_2O_2$  and  
470 ferro-hydroxy complex produced by electrolysis. A hybrid photo-electrochemical process leads to less  
471 footprint area and higher possibility of synergy between photochemical and electrochemical reactions.  
472

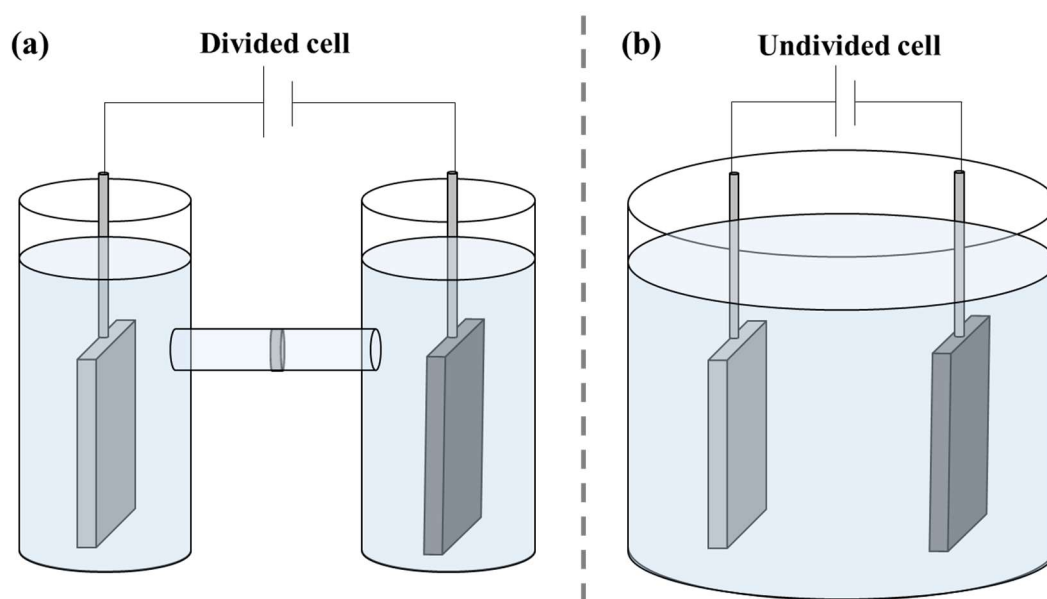
473 In contrast, the hybrid photo-electrochemical process (Figure 5b) offers many other advantages  
474 such as the low footprint area, the possibility of synergy between photochemical and  
475 electrochemical reactions according to the catalyst support as discussed in section 2.3 and to  
476 the hybrid reactor configuration as shown in the following sub-sections 3.2, 3.3 and 3.4. These

477 benefits gained from the hybrid process explain the higher number of studies selecting this  
478 configuration (Table 3).

479

### 480 3.2. Reactor configuration: divided versus undivided cells

481 In electrolysis, there are two possibilities of operation, either in divided cell (Figure 6a) or in  
482 undivided cell (Figure 6b). Considering the photo-electrochemical process implementation, the  
483 main influence of efficiency comes from the electrochemical reactions. In divided cell, the  
484 advantage is that there is the possibility to avoid decomposition of oxidants at anode or cathode  
485 which increases the faradic yield (Esquivel et al. 2009; Ramirez et al. 2015). However, some  
486 redox reactions cannot be involved in the cell such as ferrous/ferric cycle that is useful for the  
487  $\text{Fe}^{2+}$  regeneration (Eq. 3) in an electro-Fenton process for example. In contrast, this catalytic  
488 behaviour of iron species can be obtained in an undivided cell (Sirés et al. 2007). This latter  
489 configuration has been the most studied in photo-electrochemical reactors (Table 3), especially  
490 for its easier implementation at industrial scale if a stirred tank reactor is foreseen.



491

492 **Figure 6.** Divided cell (a) versus undivided cell (b) configurations for hybrid photo-electrochemical  
493 processes. Divided cell configuration avoids the decomposition of oxidants on the anode or cathode  
494 surfaces depending on the species. Practically, undivided cell is more developed and the redox cycle  
495 of iron can occur in this condition to implement Fenton reaction.

496

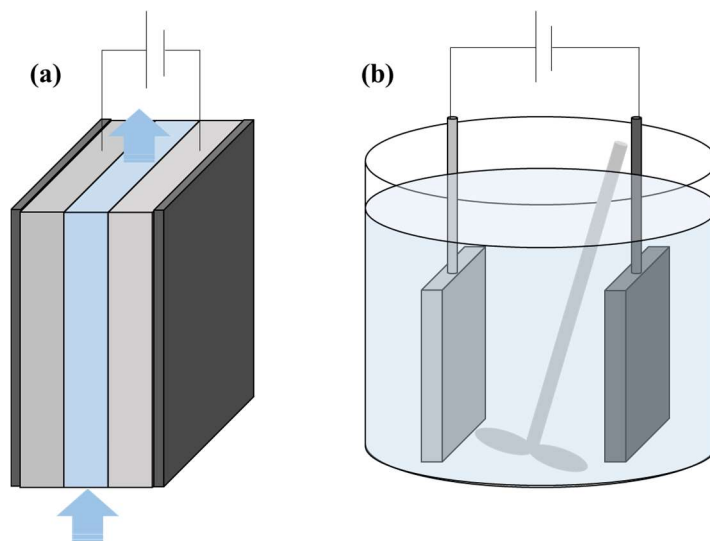
### 497 **3.3. Operation mode: flow-cell versus stirred tank reactor**

498 There are two main operation modes of photo-electrochemical reactors developed in literature  
499 (Figure 7). In the flow cell (Figure 7a), the flux is forced to go between parallel electrodes and  
500 the mode can be assimilated to a plug-flow reactor when flushed continuously. Most of the time  
501 it is operated in recirculated batch in lab scale studies. In a stirred tank reactor (Figure 7b), the  
502 electrodes are placed in parallel in a tank that is mechanically stirred (Ding et al. 2012; Zhai et  
503 al. 2013; Garcia-Segura et al. 2014; Bessegato et al. 2015; Mousset et al. 2017a). The effluent  
504 can be flushed continuously and can be ascribed to a continuous stirred tank reactor mode when  
505 the solution is assumed as perfectly mixed, i.e. the homogeneous concentration in the reactor  
506 equal the output stream.

507 A hydrodynamic characterisation has shown that parallel electrodes system in a stirred tank  
508 reactor could be modelled as an ideal single continuous stirred tank reactor at high rotational  
509 speed of the impeller with impeller Reynolds number higher than  $10^4$  (Polcaro et al., 2007).  
510 The geometry proposed in literature is either parallelepipedal (Khataee et al. 2012) or  
511 cylindrical (Ding et al. 2012; Zhai et al. 2013; Garcia-Segura et al. 2014; Bessegato et al. 2015;  
512 Mousset et al. 2017a). The latter is the most frequent shape since it limits the stagnant zone in  
513 which no mixing occurs. The drawbacks of continuous stirred tank reactor is that the mass  
514 transfer rate is lower than in flow cell (Anglada et al. 2010). This is confirmed by the  
515 comparison between a cylindrical stirred tank reactor of 0.1 L and a flow-by cell with a reservoir  
516 tank of 10 L that was performed by Garcia-Segura et al. (2014). Considering the difference of  
517 electrochemical reactor volume in each kind of reactor, the time to reach 50% of  
518 chloramphenicol degradation was 26-fold higher in stirred tank reactor than in solar filter-press  
519 reactor (Garcia-Segura et al. 2014).

520 Moreover, the electrode distance can be better controlled and easily optimized in flow cells by  
521 varying it from a few tens of microns until several centimetres (Scialdone et al. 2010). It leads  
522 to better mass transport of targeted compounds towards the electrodes, with mass transport  
523 coefficient improved by two to more than ten times (Anglada et al. 2010; Mousset et al. 2019b).  
524 A high mass transport is essential to favour heterogeneous catalysis (Mousset et al. 2019a) that  
525 is involved at electrode surface in photo-electrochemical processes. Minimized electrode  
526 distances also permit the reduction of cell potential and therefore the energy requirement is  
527 reduced. The flow cell has also advantage for process scale-up since it can be arranged in series  
528 and parallel to increase the removal efficiency and the treatment capacity respectively, while

529 keeping a low footprint compared to continuous stirred tank reactor (Martínez-Huitle et al.  
530 2015).



531  
532 **Figure 7.** Flow-by cell (a) and stirred tank reactor (b) configurations for hybrid photo-electrochemical  
533 processes. The flow-by cell is assimilated to a plug-flow reactor while the stirred tank reactor is  
534 associated with the continuous stirred tank reactor model. The flow-by cell increases the mass  
535 transfers towards the electrodes compared to the stirred tank reactor, which is an advantage to  
536 implement heterogeneous catalysis and photochemical reactions.

537

### 538 3.4. Light source positioning

539 The light positioning is an important parameter in photochemical processes since the energy  
540 delivered by light irradiation decrease with the distance between the light source and the  
541 targeted compound in solution. The influence of light irradiation source placed in stirred tank  
542 reactor or in flow-cell configurations considering hybrid photo-electrochemical processes is  
543 displayed in Figure 8.

544 The light source can be placed externally of the reactor (Figures 8a-8g) and especially at the  
545 top of a stirred tank reactor with parallel electrode configuration (Garza-Campos et al. 2014)  
546 (Figure 8a) or with one vertical electrode and one horizontal electrode that contain the  
547 photocatalyst (Daskalaki et al. 2013) (Figure 8b) in order to improve the contact between the  
548 light and photocatalyst. In this latter case, the light can also be shined at the bottom of the stirred  
549 tank reactor (Xie and Li 2006) (Figure 8b) through the reactor in order to minimize the distance  
550 between the light and the horizontal photo-electrode. It is important to highlight that quartz  
551 reactors are preferred instead of glass reactors, since the transmittance of quartz material is very  
552 high for a wide range of wavelength, even in UV region (Mousset et al. 2017a).

553 Another possibility is to let shine the light across the side of the stirred tank reactor (Figure 8c)  
554 and either enhance the H<sub>2</sub>O<sub>2</sub> photolysis by being close to the carbon cathode (Mousset et al.  
555 2017a) or improve the photoelectrocatalysis performance using a transparent photo-anode  
556 (Mousset et al. 2017a). This latter option has been proposed to be implemented in a semi-  
557 cylindrical reactor in which the transparent photo-anode is placed against the flat side (Ding et  
558 al. 2012) (Figure 8d) in order to optimize the distance between the light and the photo-anode.  
559 This distance is even better optimized in flow-cell systems in which interelectrode distance can  
560 be easily reduced as discussed in section 3.3. In this configuration, the light is usually shined  
561 through a mesh electrode (Catanho et al. 2006) (Figure 8e) or a transparent electrode (Figure  
562 8f) using an external transparent wall.

563 More recently, it has been proposed to make full use of light energy by letting shine the light  
564 directly across a transparent anode material (Mousset et al. 2017a) (Figure 8g), named fluorine-  
565 doped tin oxide. This customized configuration could be obtained by additive manufacturing,  
566 avoiding the use of quartz material that is expensive and fragile. The proposed three  
567 dimensional-printed reactor design allowed for 1.87 times increase of efficiency of photo-based  
568 processes involved in the reactor as compared to a continuous stirred tank reactor system.  
569 Moreover, the use of fluorine-doped tin oxide offers the advantage of being a high O<sub>2</sub>  
570 overvoltage anode reaching a potential of 2.1 V (Mousset et al. 2017a), which constitutes  
571 another source of <sup>•</sup>OH production for electrochemical advanced oxidation processes  
572 combination with photocatalysis or photoelectrocatalysis.

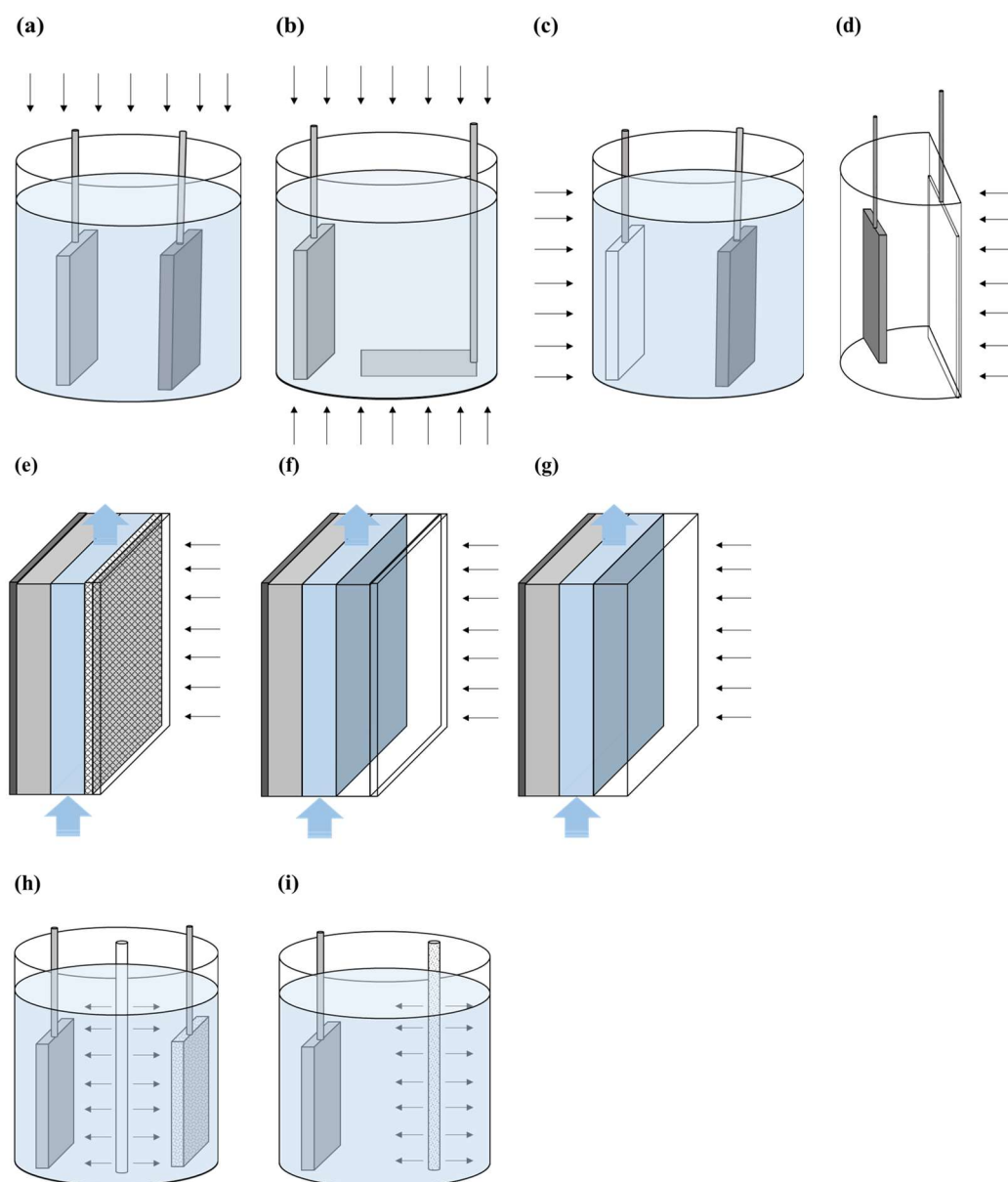
573  
574 Immersed light positioning systems have also been considered (Bessegato et al., 2015; Esquivel  
575 et al., 2009; Khataee et al., 2012) (Figures 8h, 8i). The source can be placed close to the cathode  
576 and the anode in order to favour the photocatalysis mechanism combined with electrolysis  
577 (Khataee et al. 2012; Bessegato et al. 2015) (Figure 8h). A second option is to use a source such  
578 as optical fibre that is coated with a photocatalyst and employed as a photo-anode connected to  
579 a cathode (Esquivel et al. 2009) (Figure 8i). In this latter case, the photoelectrocatalysis is  
580 implemented and can be combined to electrochemical advanced oxidation processes  
581 technologies for a better pollutant removal efficiency than electrochemical advanced  
582 oxidation/photocatalysis processes combination, as discussed in section 2.3.

583 It is necessary to note that when a transparent material is used to involve photocatalysis or  
584 photoelectrocatalysis in a light-through electrolytic system, there is an optimal photocatalyst  
585 loading. It depends on several factors such as optical properties of the catalyst, e.g. optical

586 thickness and transmittance, and of the transparent substrate material as well as photocatalyst  
587 particle size (Hurtado et al., 2015; Motegh et al., 2012; Murakami et al., 2012). For instance, it  
588 has been shown that a transmittance of 20%, corresponding to a dose of  $0.31 \text{ mg cm}^{-2}$  of  $\text{TiO}_2$   
589 (P-25) coated on a glass/fluorine-doped tin oxide transparent material, was found optimal for a  
590 maximum pollutant removal efficiency in a hybrid photo-electrochemical reactor (Mousset et  
591 al. 2017a).

592

593 Another important point is that the use of solar light as irradiation source is decisive in the  
594 position of electrodes in the reactor and in the reactor design as well. Since the solar light is  
595 coming from the top, compound parabolic concentrators oriented towards the sun have been  
596 developed to maximize the quantum yield and have been combined with electrolysis cells  
597 (Garcia-Segura et al. 2014). Solar light was used as free energy source in photoelectrochemical  
598 systems and could successfully reduce the operating costs while keeping very high removal  
599 yield as compared to artificial light (El-Ghenymy et al. 2012, 2013; Garcia-Segura and Brillas  
600 2014).



601  
 602 **Figure 8.** Influence of light irradiation source placed externally of the reactor ((a)-(g)) or immersed  
 603 ((h), (i)), in stirred tank reactor ((a)-(d), (h), (i)) and in flow-cell ((e), (f), (g)) configurations  
 604 considering hybrid photo-electrochemical processes. If an external source is implemented on the side  
 605 or at the bottom of the reactor, the reactor material needs to be suitable for allowing UV radiation to  
 606 pass through. Such material is quartz that is very fragile and expensive. When the light is implemented  
 607 in a stirred tank reactor, the distance between the light source and the electrode needs to be minimized  
 608 for better synergy and maximum quantum yields. Flow-cell allows varying the interelectrode gap from  
 609 micro-distance (50-500  $\mu\text{m}$ ) to macro-distance (1-5 cm), which can easily permit optimisation of the  
 610 penetration depth when light is applied through the cell.

## 611 **4. Conclusion**

612 Studies on photo-electrochemical reactors applied for advanced oxidation treatment of  
613 wastewater are still at early stages though increasing attention is being devoted to this  
614 technology. This chapter presented an overview of the possible synergetic combinations  
615 between advanced electrochemical treatments and photochemical processes. The effect of  
616 reactor design, i.e. sequential versus hybrid photo-reactors, divided versus undivided cells,  
617 operation mode, i.e. flow cell versus stirred tank reactors, and light source positioning, on the  
618 photo-reactors efficiency has been addressed. The synergy between photoelectrocatalysis and  
619 electrochemical advanced oxidation processes seems promising in terms of removal efficiency  
620 of organic pollutants.

621 Upon these preliminary results, there is a need to manufacture multifunctional electrode  
622 materials possessing optimum properties and configuration for the design/development of  
623 heterogeneous photocatalytic reactors with enhanced performance. In parallel, the  
624 photocatalysts have to be developed so they can possess long-term activity and improved  
625 coating stability, particularly when subjected to electric field.

626 Furthermore, most studies from literature are performed at laboratory scale while most of the  
627 effluents tested are synthetic solutions. There is a need to upscale those processes by testing  
628 real water matrix solutions. The pH, the temperature, the turbidity, the presence of organic  
629 matter as well as the inorganic salts could interfere with the combined process efficiency. A  
630 techno-economic study could then be assessed for comparison with commercialized  
631 technologies.

632

## 633 **References**

634 Alcántara MT, Gómez J, Pazos M, Sanromán MA (2009) PAHs soil decontamination in two  
635 steps: desorption and electrochemical treatment. *J Hazard Mater* 166:462–468. doi:  
636 10.1016/j.jhazmat.2008.11.050

637 Almazán-Sánchez PT, Cotillas S, Sáez C, et al (2017) Removal of pendimethalin from soil  
638 washing effluents using electrolytic and electro-irradiated technologies based on diamond  
639 anodes. *Appl Catal B Environ* 213:190–197. doi: 10.1016/j.apcatb.2017.05.008

640 Andersen J, Han C, O’Shea K, Dionysiou DD (2014) Revealing the degradation intermediates  
641 and pathways of visible light-induced NF-TiO<sub>2</sub> photocatalysis of microcystin-LR. *Appl*

642 Catal B Environ 154–155:259–266. doi: 10.1016/j.apcatb.2014.02.025

643 Anglada A, Urtiaga AM, Ortiz I (2010) Laboratory and pilot plant scale study on the  
644 electrochemical oxidation of landfill leachate. *J Hazard Mater* 181:729–35. doi:  
645 10.1016/j.jhazmat.2010.05.073

646 Aquino JM, Rocha-Filho RC, Ruotolo LAM, et al (2014) Electrochemical degradation of a real  
647 textile wastewater using  $\beta$ -PbO<sub>2</sub> and DSA<sup>®</sup> anodes. *Chem Eng J* 251:138–145. doi:  
648 10.1016/j.cej.2014.04.032

649 Araújo DM de, Sáez C, Martínez-Huitle CA, et al (2015) Influence of mediated processes on  
650 the removal of Rhodamine with conductive-diamond electrochemical oxidation. *Appl*  
651 *Catal B Environ* 166–167:454–459. doi: 10.1016/j.apcatb.2014.11.038

652 Barndök H, Hermosilla D, Han C, et al (2016) Degradation of 1,4-dioxane from industrial  
653 wastewater by solar photocatalysis using immobilized NF-TiO<sub>2</sub> composite with  
654 monodisperse TiO<sub>2</sub> nanoparticles. *Appl Catal B Environ* 180:44–52. doi:  
655 10.1016/j.apcatb.2015.06.015

656 Bergmann MEH, Rollin J, Iourtchouk T (2009) The occurrence of perchlorate during drinking  
657 water electrolysis using BDD anodes. *Electrochim Acta* 54:2102–2107. doi:  
658 10.1016/j.electacta.2008.09.040

659 Besnault S, Martin S (2011) Etat de l'art sur les procédés avancés intensifs pour la réduction  
660 de micropolluants dans les eaux usées traitées. Rapport bibliographique (French).  
661 [https://professionnels.afbiodiversite.fr/sites/default/files/pdf/2011\\_039.pdf](https://professionnels.afbiodiversite.fr/sites/default/files/pdf/2011_039.pdf)

662 Bessegato GG, Cardoso JC, Zanoni MVB (2015) Enhanced photoelectrocatalytic degradation  
663 of an acid dye with boron-doped TiO<sub>2</sub> nanotube anodes. *Catal Today* 240:100–106. doi:  
664 10.1016/j.cattod.2014.03.073

665 Brillas E, Boye B, Dieng MM (2003) Peroxi-coagulation and photoperoxi-coagulation  
666 treatments of the herbicide 4-chlorophenoxyacetic acid in aqueous medium using an  
667 oxygen-diffusion cathode. *J Electrochem Soc* 150:E148–E154. doi: 10.1149/1.1543950

668 Brillas E, Martinez-Huitle CA (2011) Synthetic diamond films: preparation, electrochemistry,  
669 characterization, and applications. Wiley, New Jersey. doi:10.1002/9781118062364

670 Brillas E, Martínez-Huitle CA (2015) Decontamination of wastewaters containing synthetic  
671 organic dyes by electrochemical methods. An updated review. *Appl Catal B Environ* 166–  
672 167:603–643. doi: 10.1016/j.apcatb.2014.11.016

673 Brillas E, Sauleda R, Casado J (1997) Peroxi-coagulation of aniline in acidic medium using an  
674 oxygen diffusion cathode. *J Electrochem Soc* 144:2374. doi: 10.1149/1.1837821

675 Brillas E, Sirés I, Oturan MA (2009) Electro-Fenton process and related electrochemical  
676 technologies based on Fenton's reaction chemistry. *Chem Rev* 109:6570–6631. doi:  
677 10.1007/s00894-008-0358-0

678 Brito CDN, de Araújo DM, Martínez-Huitle CA, Rodrigo MA (2015) Understanding active  
679 chlorine species production using boron doped diamond films with lower and higher  
680  $sp^3/sp^2$  ratio. *Electrochem commun* 55:34–38. doi: 10.1016/j.elecom.2015.03.013

681 Catanho M, Malpass GRP, Motheo AJ (2006) Photoelectrochemical treatment of the dye  
682 reactive red 198 using DSA<sup>®</sup> electrodes. *Appl Catal B Environ* 62:193–200. doi:  
683 10.1016/j.apcatb.2005.07.011

684 Chaplin BP (2014) Critical review of electrochemical advanced oxidation processes for water  
685 treatment applications. *Environ Sci Process Impacts* 16:1182–203. doi:  
686 10.1039/c3em00679d

687 Cizmas L, Sharma VK, Gray CM, McDonald TJ (2015) Pharmaceuticals and personal care  
688 products in waters: occurrence, toxicity, and risk. *Environ Chem Lett* 13:381–394. doi:  
689 10.1007/s10311-015-0524-4

690 Comninellis C, Chen G (eds) (2010) *Electrochemistry for the environment*. Springer Nature,  
691 pp 563. doi:10.1007/978-0-387-68318-8

692 Daskalaki VM, Fulgione I, Frontistis Z, et al (2013) Solar light-induced photoelectrocatalytic  
693 degradation of bisphenol-A on TiO<sub>2</sub>/ITO film anode and BDD cathode. *Catal Today*  
694 209:74–78. doi: 10.1016/j.cattod.2012.07.026

695 Ding X, Ai Z, Zhang L (2012) Design of a visible light driven photo-electrochemical/electro-  
696 Fenton coupling oxidation system for wastewater treatment. *J Hazard Mater* 239–  
697 240:233–40. doi: 10.1016/j.jhazmat.2012.08.070

698 Ding X, Ai Z, Zhang L (2014) A dual-cell wastewater treatment system with combining anodic  
699 visible light driven photoelectro-catalytic oxidation and cathodic electro-Fenton oxidation.  
700 *Sep Purif Technol* 125:103–110. doi: 10.1016/j.seppur.2014.01.046

701 Dorfman LM, Adams GE (1973) Reactivity of the hydroxyl radical in aqueous solutions. 59  
702 pp. Accession Number : ADD095248

703 dos Santos EV, Sáez C, Cañizares P, et al (2017) Treatment of ex-situ soil-washing fluids  
704 polluted with petroleum by anodic oxidation , photolysis , sonolysis and combined  
705 approaches. *Chem Eng J* 310:581–588. doi: 10.1016/j.cej.2016.05.015

706 dos Santos EV, Saez C, Martinez-Huitle CA, et al (2015) Combined soil washing and CDEO  
707 for the removal of atrazine from soils. *J Hazard Mater* 300:129–134. doi:

708 10.1016/j.jhazmat.2015.06.064  
709 dos Santos EV, Scialdone O (2018) Photo-electrochemical technologies for removing organic  
710 compounds in wastewater, *Electrochemical water and wastewater treatment*. Elsevier, pp.  
711 239-266. doi:10.1016/B978-0-12-813160-2.00010-9.  
712 El-Ghenymy A, Cabot PL, Centellas F, et al (2013) Mineralization of sulfanilamide by electro-  
713 Fenton and solar photoelectro-Fenton in a pre-pilot plant with a Pt/air-diffusion cell.  
714 *Chemosphere* 91:1324–31. doi: 10.1016/j.chemosphere.2013.03.005  
715 El-Ghenymy A, Garcia-Segura S, Rodríguez RM, et al (2012) Optimization of the electro-  
716 Fenton and solar photoelectro-Fenton treatments of sulfanilic acid solutions using a pre-  
717 pilot flow plant by response surface methodology. *J Hazard Mater* 221–222:288–97. doi:  
718 10.1016/j.jhazmat.2012.04.053  
719 Esquivel K, Arriaga LG, Rodríguez FJ, et al (2009) Development of a TiO<sub>2</sub> modified optical  
720 fiber electrode and its incorporation into a photoelectrochemical reactor for wastewater  
721 treatment. *Water Res* 43:3593–3603. doi: 10.1016/j.watres.2009.05.035  
722 Fagan R, McCormack DE, Dionysiou DD, Pillai SC (2016) A review of solar and visible light  
723 active TiO<sub>2</sub> photocatalysis for treating bacteria, cyanotoxins and contaminants of  
724 emerging concern. *Mater Sci Semicond Process* 42:2–14. doi:  
725 10.1016/j.mssp.2015.07.052  
726 Fang T, Yang C, Liao L (2012) Photoelectrocatalytic degradation of high COD dipterex  
727 pesticide by using TiO<sub>2</sub>/Ni photo electrode. *J Environ Sci (China)* 24:1149–1156. doi:  
728 10.1016/S1001-0742(11)60882-6  
729 Faust BC, Hoigné J (1990) Photolysis of Fe (III)-hydroxy complexes as sources of OH radicals  
730 in clouds, fog and rain. *Atmos Environ Part A, Gen Top* 24:79–89. doi: 10.1016/0960-  
731 1686(90)90443-Q  
732 Feng L, van Hullebusch ED, Rodrigo MA, et al (2013) Removal of residual anti-inflammatory  
733 and analgesic pharmaceuticals from aqueous systems by electrochemical advanced  
734 oxidation processes. A review. *Chem Eng J* 228:944–964  
735 Fujishima A, Rao TN, Tryk DA (2000) Titanium dioxide photocatalysis. *J Photochem*  
736 *Photobiol C Photochem Rev* 1:1–21. doi: 10.1016/S1389-5567(00)00002-2  
737 Ganiyu SO, Oturan N, Raffy S, et al (2016) Sub-stoichiometric titanium oxide (Ti<sub>4</sub>O<sub>7</sub>) as a  
738 suitable ceramic anode for electrooxidation of organic pollutants: A case study of kinetics,  
739 mineralization and toxicity assessment of amoxicillin. *Water Res* 106:171–182. doi:  
740 10.1016/j.watres.2016.09.056

741 Ganiyu SO, Oturan N, Raffy S, et al (2017) Use of sub-stoichiometric titanium oxide as a  
742 ceramic electrode in anodic oxidation and electro-Fenton degradation of the beta-blocker  
743 propranolol: Degradation kinetics and mineralization pathway. *Electrochim Acta*  
744 242:344–354. doi: 10.1016/j.electacta.2017.05.047

745 Ganiyu SO, Zhou M, Martínez-huitle CA (2018) Heterogeneous electro-Fenton and  
746 photoelectro-Fenton processes: A critical review of fundamental principles and  
747 application for water/wastewater treatment. *Appl Catal B Environ* 235:103–129. doi:  
748 10.1016/j.apcatb.2018.04.044

749 Ganzenko O, Oturan N, Sirés I, et al (2018) Fast and complete removal of the 5-fluorouracil  
750 drug from water by electro-Fenton oxidation. *Environ Chem Lett* 16:281–286. doi:  
751 10.1007/s10311-017-0659-6

752 Garcia-Rodriguez O, Lee YY, Olvera-Vargas H, et al (2018) Mineralization of electronic  
753 wastewater by electro-Fenton with an enhanced graphene-based gas diffusion cathode.  
754 *Electrochim Acta* 276:12–20. doi: 10.1016/j.electacta.2018.04.076

755 Garcia-Segura S, Brillas E (2014) Advances in solar photoelectro-Fenton: Decolorization and  
756 mineralization of the Direct Yellow 4 diazo dye using an autonomous solar pre-pilot plant.  
757 *Electrochim Acta* 140:384–395. doi: 10.1016/j.electacta.2014.04.009

758 Garcia-Segura S, Cavalcanti EB, Brillas E (2014) Mineralization of the antibiotic  
759 chloramphenicol by solar photoelectro-Fenton. From stirred tank reactor to solar pre-pilot  
760 plant. *Appl Catal B Environ* 144:588–598. doi: 10.1016/j.apcatb.2013.07.071

761 Garcia-Segura S, Dosta S, Guilemany JM, Brillas E (2013) Solar photoelectrocatalytic  
762 degradation of Acid Orange 7 azo dye using a highly stable TiO<sub>2</sub> photoanode synthesized  
763 by atmospheric plasma spray. *Appl Catal B Environ* 132–133:142–150. doi:  
764 10.1016/j.apcatb.2012.11.037

765 Garza-Campos B, Brillas E, Hernandez-Ramirez A, et al (2016) Salicylic acid degradation by  
766 advanced oxidation processes. Coupling of solar photoelectro-Fenton and solar  
767 heterogeneous photocatalysis. *J Hazard Mater* 319:34–42. doi:  
768 10.1016/j.jhazmat.2016.02.050

769 Garza-Campos BR, Guzmán-Mar JL, Reyes LH, et al (2014) Coupling of solar photoelectro-  
770 Fenton with a BDD anode and solar heterogeneous photocatalysis for the mineralization  
771 of the herbicide atrazine. *Chemosphere* 97:26–33. doi:  
772 10.1016/j.chemosphere.2013.10.044

773 Glaze WH, Kang JW, Chapin DH (1987) The chemistry of water-treatment processes involving

774 ozone, hydrogen-peroxide and ultraviolet-radiation. *Ozone Sci Eng* 9:335–352.

775 Gligorovski S, Streckowski R, Barbati S, Vione D (2015) Environmental implications of  
776 hydroxyl radicals ( $\bullet\text{OH}$ ). *Chem Rev* 115:13051–13092. doi: 10.1021/cr500310b

777 Goldstein S, Aschengrau D, Diamant Y, Rabani J (2007) Photolysis of aqueous  $\text{H}_2\text{O}_2$ : Quantum  
778 yield and applications for polychromatic UV actinometry in photoreactors. *Environ Sci*  
779 *Technol* 41:7486–7490. doi: 10.1021/es071379t

780 Khataee AR, Safarpour M, Zarei M, Aber S (2012) Combined heterogeneous and homogeneous  
781 photodegradation of a dye using immobilized  $\text{TiO}_2$  nanophotocatalyst and modified  
782 graphite electrode with carbon nanotubes. *J Mol Catal A Chem* 363–364:58–68. doi:  
783 10.1016/j.molcata.2012.05.016

784 Lahkimi A, Oturan MA, Oturan N, Chaouch M (2007) Removal of textile dyes from water by  
785 the electro-Fenton process. *Environ Chem Lett* 5:35–39. doi: 10.1007/s10311-006-0058-  
786 x

787 Lazar M, Varghese S, Nair S (2012) Photocatalytic water treatment by titanium dioxide: Recent  
788 updates. *Catalysts* 2:572–601. doi: 10.3390/catal2040572

789 Le TXH, Bechelany M, Lacour S, et al (2015a) High removal efficiency of dye pollutants by  
790 electron-Fenton process using a graphene based cathode. *Carbon N Y* 94:1003–1011. doi:  
791 10.1016/j.carbon.2015.07.086

792 Le TXH, Bechelany M, Champavert J, Cretin M (2015b) A highly active based graphene  
793 cathode for electro-Fenton reaction. *RSC Adv* 5:42536–42539.  
794 doi:10.1039/C5RA04811G

795 Le TXH, Charmette C, Bechelany M, Cretin M (2016) Facile preparation of porous carbon  
796 cathode to eliminate paracetamol in aqueous medium using electro-Fenton system.  
797 *Electrochim Acta* 188:378–384. doi: 10.1016/j.electacta.2015.12.005

798 Liu X, Zhang H, Liu C, et al (2014) UV and visible light photoelectrocatalytic bactericidal  
799 performance of 100% {1 1 1} faceted rutile  $\text{TiO}_2$  photoanode. *Catal Today* 224:77–82.  
800 doi: 10.1016/j.cattod.2013.09.041

801 Liu Y, Li J, Zhou B, et al (2009) Comparison of photoelectrochemical properties of  $\text{TiO}_2$ -  
802 nanotube-array photoanode prepared by anodization in different electrolyte. *Environ*  
803 *Chem Lett* 7:363–368. doi: 10.1007/s10311-008-0180-z

804 Luo H, Li C, Wu C, et al (2015) Electrochemical degradation of phenol by in situ electro-  
805 generated and electro-activated hydrogen peroxide using an improved gas diffusion  
806 cathode. *Electrochim Acta* 186:486–493. doi: 10.1016/j.electacta.2015.10.194

807 Luo Y, Guo W, Ngo HH, et al (2014) A review on the occurrence of micropollutants in the  
808 aquatic environment and their fate and removal during wastewater treatment. *Sci Total*  
809 *Environ* 473–474:619–41. doi: 10.1016/j.scitotenv.2013.12.065

810 Malato S, Fernandez-Ibanez P, Maldonado MI, et al (2009) Decontamination and disinfection  
811 of water by solar photocatalysis: Recent overview and trends. *Catal Today* 147:1–59. doi:  
812 10.1016/j.cattod.2009.06.018

813 Martínez-Huitle CA, Brillas E (2009) Decontamination of wastewaters containing synthetic  
814 organic dyes by electrochemical methods: A general review. *Appl. Catal. B Environ.*  
815 87:105–145.

816 Martínez-Huitle CA, Rodrigo MA, Sirés I, Scialdone O (2015) Single and coupled  
817 electrochemical processes and reactors for the abatement of organic water pollutants: A  
818 critical review. *Chem Rev* 115:13362–13407. doi: 10.1021/acs.chemrev.5b00361

819 Merényi G, Lind J, Naumov S, Sonntag C von (2010) Reaction of ozone with hydrogen  
820 peroxide (peroxone process): A revision of current mechanistic concepts based on  
821 thermokinetic and quantum-chemical considerations. *Environ Sci Technol* 44:3505–7.  
822 doi: 10.1021/es100277d

823 Moreira FC, Boaventura RAR, Brillas E, Vilar VJP (2017) Electrochemical advanced oxidation  
824 processes: A review on their application to synthetic and real wastewaters. *Appl Catal B*  
825 *Environ* 202:217–261. doi: 10.1016/j.apcatb.2016.08.037

826 Mousset E, Frunzo L, Esposito G, et al (2016a) A complete phenol oxidation pathway obtained  
827 during electro-Fenton treatment and validated by a kinetic model study. *Appl Catal B*  
828 *Environ* 180:189–198.

829 Mousset E, Huang Weiqi V, Foong Yang Kai B, et al (2017a) A new 3D-printed  
830 photoelectrocatalytic reactor combining the benefits of a transparent electrode and the  
831 Fenton reaction for advanced wastewater treatment. *J Mater Chem A* 5:24951–24964. doi:  
832 10.1039/C7TA08182K

833 Mousset E, Huguenot D, Van Hullebusch ED, et al (2016b) Impact of electrochemical treatment  
834 of soil washing solution on PAH degradation efficiency and soil respirometry. *Environ*  
835 *Pollut* 211:354–362. doi: 10.1016/j.envpol.2016.01.021

836 Mousset E, Ko ZT, Syafiq M, et al (2016c) Electrocatalytic activity enhancement of a graphene  
837 ink-coated carbon cloth cathode for oxidative treatment. *Electrochim Acta* 222:1628–  
838 1641. doi: 10.1016/j.electacta.2016.11.151

839 Mousset E, Oturan N, Oturan MA (2018a) An unprecedented route of OH radical reactivity

840 evidenced by an electrocatalytical process: Ipso-substitution with perhalogenocarbon  
841 compounds. *Appl Catal B Environ* 226:135–146. doi: 10.1016/j.apcatb.2017.12.028

842 Mousset E, Oturan N, van Hullebusch ED, et al (2013) A new micelle-based method to quantify  
843 the Tween 80<sup>®</sup> surfactant for soil remediation. *Agron Sustain Dev* 33:839–846. doi:  
844 10.1007/s13593-013-0140-2

845 Mousset E, Oturan N, van Hullebusch ED, et al (2014a) Influence of solubilizing agents  
846 (cyclodextrin or surfactant) on phenanthrene degradation by electro-Fenton process -  
847 Study of soil washing recycling possibilities and environmental impact. *Water Res*  
848 48:306–316. doi: 10.1016/j.watres.2013.09.044

849 Mousset E, Oturan N, van Hullebusch ED, et al (2014b) Treatment of synthetic soil washing  
850 solutions containing phenanthrene and cyclodextrin by electro-oxidation. Influence of  
851 anode materials on toxicity removal and biodegradability enhancement. *Appl Catal B*  
852 *Environ* 160–161:666–675. doi: 10.1016/j.apcatb.2014.06.018

853 Mousset E, Pechaud Y, Oturan N, Oturan MA (2019a) Charge transfer/mass transport  
854 competition in advanced hybrid electrocatalytic wastewater treatment: Development of a  
855 new current efficiency relation. *Appl Catal B Environ* 240:102–111. doi:  
856 10.1016/j.apcatb.2018.08.055

857 Mousset E, Pontvianne S, Pons M-N (2018b) Fate of inorganic nitrogen species under  
858 homogeneous Fenton combined with electro-oxidation/reduction treatments in synthetic  
859 solutions and reclaimed municipal wastewater. *Chemosphere* 201:6–12. doi:  
860 10.1016/j.chemosphere.2018.02.142

861 Mousset E, Puce M, Pons M-N (2019b) Advanced electro-oxidation with boron-doped diamond  
862 for acetaminophen removal from real wastewater in a microfluidic reactor – Kinetics and  
863 mass transfer studies. *ChemElectroChem* 6:2908–2916. doi: 10.1002/celec.201900182

864 Mousset E, Quackenbush L, Schondek C, et al (2020) Effect of homogeneous Fenton combined  
865 with electron transfer on the fate of inorganic chlorinated species in synthetic and  
866 reclaimed municipal wastewater. *Electrochim Acta*. doi: 10.1016/j.electacta.2019.135608

867 Mousset E, Wang Z, Hammaker J, Lefebvre O (2017b) Electrocatalytic phenol degradation by  
868 a novel nanostructured carbon fiber brush cathode coated with graphene ink. *Electrochim*  
869 *Acta*. doi: 10.1016/j.electacta.2017.11.104

870 Mousset E, Wang Z, Hammaker J, Lefebvre O (2016d) Physico-chemical properties of pristine  
871 graphene and its performance as electrode material for electro-Fenton treatment of  
872 wastewater. *Electrochim Acta* 214:217–230. doi: 10.1016/j.electacta.2016.08.002

873 Mousset E, Wang Z, Lefebvre O (2016e) Electro-Fenton for control and removal of  
874 micropollutants - Process optimization and energy efficiency. *Water Sci Technol*  
875 74:2068–2074. doi:10.2166/wst.2016.353

876 Mousset E, Zhou M (2017) Graphene-based nanostructured materials for advanced  
877 electrochemical water/wastewater treatment. In: Thomas S, Thankappan A (eds)  
878 Polymeric and nanostructured materials: Synthesis, properties and advanced applications,  
879 Apple Acad. pp. 321–358. ISBN:9781771886444

880 Nidheesh PV. (2018) Removal of organic pollutants by peroxicoagulation. *Environ Chem Lett*  
881 16:1283–1292. doi: 10.1007/s10311-018-0752-5

882 Oturan MA, Aaron J-J (2014) Advanced oxidation processes in water/wastewater treatment:  
883 Principles and applications. A Review. *Crit Rev Environ Sci Technol* 44:2577–2641. doi:  
884 10.1080/10643389.2013.829765

885 Oturan N, Brillas E, Oturan MA (2012) Unprecedented total mineralization of atrazine and  
886 cyanuric acid by anodic oxidation and electro-Fenton with a boron-doped diamond anode.  
887 *Environ Chem Lett* 10:165–170. doi: 10.1007/s10311-011-0337-z

888 Panizza M, Cerisola G (2009) Direct and mediated anodic oxidation of organic pollutants.  
889 *Chem Rev* 109:6541–6569. doi: 10.1021/cr9001319

890 Panizza M, Martinez-Huitle CA (2013) Role of electrode materials for the anodic oxidation of  
891 a real landfill leachate--comparison between Ti-Ru-Sn ternary oxide, PbO<sub>2</sub> and boron-  
892 doped diamond anode. *Chemosphere* 90:1455–60. doi:  
893 10.1016/j.chemosphere.2012.09.006

894 Pelaez M, Nolan NT, Pillai SC, et al (2012) A review on the visible light active titanium dioxide  
895 photocatalysts for environmental applications. *Appl Catal B Environ* 125:331–349. doi:  
896 10.1016/j.apcatb.2012.05.036

897 Ramirez RJ, Pineda CA, Álvarez AA, et al (2015) H<sub>2</sub>O<sub>2</sub>-assisted TiO<sub>2</sub> generation during the  
898 photoelectrocatalytic process to decompose the acid green textile dye by Fenton reaction.  
899 *J Photochem Photobiol A Chem* 305:51–59. doi: 10.1016/j.jphotochem.2015.03.004

900 Ren G, Zhou M, Su P, et al (2018) Highly energy-efficient removal of acrylonitrile by peroxi-  
901 coagulation with modified graphite felt cathode: influence factors, possible mechanism.  
902 *Chem Eng J* 343:467–476. doi:10.1016/j.cej.2018.02.115

903 Schneider J, Matsuoka M, Takeuchi M, et al (2014) Understanding TiO<sub>2</sub> photocatalysis:  
904 Mechanisms and materials. *Chem Rev* 114:9919–9986. doi: 10.1021/cr5001892

905 Scialdone O, Guarisco C, Galia A, et al (2010) Anodic abatement of organic pollutants in water

906 in micro reactors. *J Electroanal Chem* 638:293–296. doi: 10.1016/j.jelechem.2009.10.031  
907 Shi H, Ni J, Zheng T, et al (2020) Remediation of wastewater contaminated by antibiotics. A  
908 review. *Environ Chem Lett* 18:345–360. doi: 10.1007/s10311-019-00945-2  
909 Shukla S, Oturan MA (2015) Dye removal using electrochemistry and semiconductor oxide  
910 nanotubes. *Environ Chem Lett* 13:157–172. doi: 10.1007/s10311-015-0501-y  
911 Sirés I, Brillas E, Oturan MA, et al (2014) Electrochemical advanced oxidation processes:  
912 Today and tomorrow. A review. *Environ Sci Pollut Res* 21:8336–8367. doi:  
913 10.1007/s11356-014-2783-1  
914 Sirés I, Garrido JA, Rodríguez RM, et al (2007) Catalytic behavior of the Fe<sup>3+</sup>/Fe<sup>2+</sup> system in  
915 the electro-Fenton degradation of the antimicrobial chlorophene. *Appl Catal B Environ*  
916 72:382–394. doi: 10.1016/j.apcatb.2006.11.016  
917 Sopaj F (2013) Study of the influence of electrode material in the application of electrochemical  
918 advanced oxidation processes to removal of pharmaceutical pollutants from water.  
919 University of Paris-Est. <https://tel.archives-ouvertes.fr/tel-00985537>  
920 Stefan MI (ed) (2017) Advanced oxidation processes for water treatment: fundamentals and  
921 applications. IWA Publishing, London, UK. ISBN13:9781780407180  
922 Sun Y, Pignatello JJ (1993) Photochemical reactions involved in the total mineralization of 2,4-  
923 D by iron(3+)/hydrogen peroxide/UV. *Environ Sci Technol* 27:304–310. doi:  
924 10.1021/es00039a010  
925 UNESCO (2017) Wastewater, The Untapped Resource. United Nations World Water  
926 Development Report. ([http://www.unesco.org/new/en/natural-](http://www.unesco.org/new/en/natural-sciences/environment/water/wwap/wwdr/2017-wastewater-the-untapped-resource/)  
927 [sciences/environment/water/wwap/wwdr/2017-wastewater-the-untapped-resource/](http://www.unesco.org/new/en/natural-sciences/environment/water/wwap/wwdr/2017-wastewater-the-untapped-resource/))  
928 Vasudevan S, Oturan MA (2014) Electrochemistry: As cause and cure in water pollution-an  
929 overview. *Environ Chem Lett* 12:97–108. doi: 10.1007/s10311-013-0434-2  
930 Von Sonntag C (2008) Advanced oxidation processes: Mechanistic aspects. *Water Sci Technol*  
931 58:1015–1021. doi: 10.2166/wst.2008.467  
932 Xie YB, Li XZ (2006) Interactive oxidation of photoelectrocatalysis and electro-Fenton for azo  
933 dye degradation using TiO<sub>2</sub>-Ti mesh and reticulated vitreous carbon electrodes. *Mater*  
934 *Chem Phys* 95:39–50. doi: 10.1016/j.matchemphys.2005.05.048  
935 Xu Z, Li X, Li J, et al (2013) Effect of CoOOH loading on the photoelectrocatalytic  
936 performance of WO<sub>3</sub> nanorod array film. *Appl Surf Sci* 284:285–290. doi:  
937 10.1016/j.apsusc.2013.07.095  
938 Yu F, Zhou M, Yu X (2015) Cost-effective electro-Fenton using modified graphite felt that

939 dramatically enhanced on H<sub>2</sub>O<sub>2</sub> electro-generation without external aeration. *Electrochim*  
940 *Acta* 163:182–189. doi: 10.1016/j.electacta.2015.02.166

941 Zhai C, Zhu M, Ren F, et al (2013) Enhanced photoelectrocatalytic performance of titanium  
942 dioxide/carbon cloth based photoelectrodes by graphene modification under visible-light  
943 irradiation. *J Hazard Mater* 263 Pt 2:291–8. doi: 10.1016/j.jhazmat.2013.09.013

944 Zhao X, Liu H, Qu J (2010) Photoelectrocatalytic degradation of organic contaminant at hybrid  
945 BDD-ZnWO<sub>4</sub> electrode. *Catal Commun* 12:76–79. doi: 10.1016/j.catcom.2010.08.013

946 Zhao X, Qu J, Liu H, et al (2009) Photoelectrochemical degradation of anti-inflammatory  
947 pharmaceuticals at Bi<sub>2</sub>MoO<sub>6</sub>-boron-doped diamond hybrid electrode under visible light  
948 irradiation. *Appl Catal B Environ* 91:539–545. doi: 10.1016/j.apcatb.2009.06.025

949 Zhou B, Zhao X, Liu H, et al (2010) Visible-light sensitive cobalt-doped BiVO<sub>4</sub> (Co-BiVO<sub>4</sub>)  
950 photocatalytic composites for the degradation of methylene blue dye in dilute aqueous  
951 solutions. *Appl Catal B Environ* 99:214–221. doi: 10.1016/j.apcatb.2010.06.022

952 Zhou L, Zhou M, Hu Z, et al (2014) Chemically modified graphite felt as an efficient cathode  
953 in electro-Fenton for p-nitrophenol degradation. *Electrochim Acta* 140:376–383. doi:  
954 10.1016/j.electacta.2014.04.090

955